PLASMA SPECTROCHEMISTRY WITH A FOURIER TRANSFORM SPECTROMETER

BY

THOMAS JOSEPH JOHN MANNING

A DISSERTATION PRESENTED TO THE GRADUATE SCHOOL
OF THE UNIVERSITY OF FLORIDA IN
PARTIAL FULFILLMENT OF THE REQUIREMENTS
FOR THE DEGREE OF DOCTOR OF PHILOSOPHY

UNIVERSITY OF FLORIDA

1990

UNIVERSITY OF FLORIDA LIBRARIES

To my family; mother, father, brother, sister,
grandparents; whose support, love, patience,
and caring made this possible.

ACKNOWLEDGEMENTS

I would like to express my extreme gratitude to the following people whose help dedication, friendship, honesty, and loyalty made this work possible.

My family played a tremendous role in my recent success. My mother has been a source of inspiration with her hard work (teaching, Clemson) and working through her lung problems. She always asks me the question, "and what does the much mean," I wish I could say much more to express my gratitude and love. My father has dedicated his life to his family, and through his encouragement and prodding, my life has progressed at a rate which he can take much of the credit for. My parents have blessed me with good health, a good education, good morals, and the ability to dream and create with the best of them.

My sister has long been a stabilizing factor in the family and her husband, George, a welcome addition. Patrick is young, cute, impressionable, and has a great arm. Jim, my big brother, has turned out to be a good brother, someone I can count on and talk to when needed.

My grandparents, particularly my grandfather who recently passed away, are sorely missed. I can picture them talking to

friends, on a stoop or in a hall way, in Brooklyn. Bragging about their grandson, the doctor. I have come to realize that obtaining a goal of this nature is done as much for others that you care about, so that they are proud, as it is a selfish goal to satisfy your curiosity about what you are and what you can be.

Susan and Jeanne have become friends over the years. I realize my jokes were not always tactful, but they were meant to be funny. They were an outlet when the possibility existed for group politics to get out of hand.

Dr. J. D. Winefordner helped fund my salary for part of my stay at UF and gave me a the chance to discuss my ideas and experiments with him and other members of the group.

Doug Hof and Byron Palmer of the Los Alamos Fourier Transform Facility have become more than just collaborators since I first started working at LANL in 1987. I would have left UF out of frustration if it were not for the outlet they and the LAFTS provided. They let me carry out my ideas and publish my work so I could establish creditability that group politics never gave me the chance to establish. Doug and Byron showed great patience and friendship in allowing me to come back again and again to the LAFTS and for this I am truly grateful.

Lots of friends have been made in the lab who have helped me; Steve L., Tye B., Ali A., Kin N., Paul J., Andres C., Lynn P., Alicia O., Martin A., Jorge V., Barbara K., Leigh Ann F., Ed V., Ben W., Eric G., Tony M., Ramme, Nancy S., Edison B., Dennis H., Scott S., Alain B., Wellington M., and En Yu Shoa are the ones I can name right now. Jill Angus of UNM and LANL has helped me a great deal. I hope our good relationships keep up for years to come.

Arlene has recently come to play a major role in my life. Her love, caring, beauty, and outdoor lifestyle are a welcome addition to my life. I hope our relationship will be a long, full one that others will be envious of.

I thank God for Los Alamos, Byron, Doug, and my parents for sticking by me and helping me work through some tough situations. Without others, my accomplishments would be hollow if they could have been achieved at all.

TABLE OF CONTENTS

page

ACKNOWLEDGEMENTS.....iii

ABSTRACT.....viii

CHAPTER

1 INTRODUCTION.....1

2 HIGH RESOLUTION FOURIER TRANSFORM SPECTROMETER TO IDENTIFY THE ROTATIONAL STRUCTURE OF $^2\Sigma^+_g - {}^2\Sigma^+_u$ $N_2^+(0,0)$ IN A HELIUM INDUCTIVELY COUPLED PLASMA
- Introduction.....6
- Experimental.....10
- Results and Discussion.....12
- Conclusions.....14

3 A LOW FLOW ATMOSPHERIC PRESSURE NEON INDUCTIVELY COUPLED PLASMA
- Introduction.....31
- Experimental.....31
- Discussion.....33
- Conclusions.....34

4 A NONFLOWING VARIABLE GAS INDUCTIVELY COUPLED PLASMA AS A LIGHT SOURCE FOR HIGH RESOLUTION SPECTROSCOPY
- Introduction.....35
- Experimental.....36
- Results.....37
- Discussion.....38
- Conclusions.....41

5 OBSERVATIONS OF LINE SHIFTS AND LINE PROFILES IN AN INDUCTIVELY COUPLED ARGON PLASMA
- Introduction.....47
- Experimental.....50
- Results/Discussion.....52
- Conclusions.....55

6 A VARIABLE BANDPASS FILTER FOR ULTRAVIOLET AND VISIBLE FOURIER TRANSFORM SPECTROSCOPY
Introduction....84
Experimental....86
Results....88
Conclusions....88

7 AN INTENSITY, WAVENUMBER, AND RESOLUTION STANDARD FOR VISIBLE FOURIER TRANSFORM SPECTROSCOPY
Introduction....96
Experimental....97
Discussion....97
Conclusions....100

8 A SYSTEM TO STUDY NOISE IN FOURIER TRANSFORM SPECTROSCOPY
Introduction....104
Experimental....106
Results....107
Conclusions....109

9 RELATIONSHIP BETWEEN RESOLUTION AND SIGNAL-TO-NOISE RATIO'S IN FOURIER TRANSFORM SPECTROSCOPY....119

10 CONCLUSIONS....109

REFERENCES....128

BIOGRAPHICAL SKETCH....135

Abstract of Dissertation Presented to the Graduate School of the University of Florida in Partial Fulfillment of the Requirements for the Degree of Doctor of Philosophy

PLASMA SPECTROCHEMISTRY WITH A FOURIER TRANSFORM SPECTROMETER

By

Thomas Joseph John Manning

August 1990

Chairman: James D. Winefordner
Major Department: Chemistry

This dissertation can be interpreted as being two dimensional. The first dimension uses the Los Alamos Fourier Transform Spectrometer to uncover various physical aspects of a Inductively Coupled Plasma. The limits of wavenumber accuracy and resolution are pushed to measure line shifts and line profiles in an Inductively Coupled Argon Plasma. This is new physical information that the plasma spectroscopy community has been seeking for several years. Other plasma spectroscopy carried out includes line profile studies, plasma diagnostics, and exact identification of diatomic molecular spectra.

The second aspect of the dissertation involves studies of light sources for Fourier Transform Spectroscopy. Sources developed use an inductively coupled plasma (ICP) power supply. New sources (neon ICP, closed cell ICP, and helium ICP) were developed and new methods to enhance the performance and understand a Fourier Transform Spectrometer were studied including a novel optical filter, a spectrum analyzer to study noises, and a standard to calibrate and evaluate a Fourier Transform Spectrometer.

CHAPTER 1
INTRODUCTION

This dissertation will introduce new applications and studies that couple a Fourier Transform Spectrometer operating in the ultraviolet and visible region of the spectrum to various plasma and discharge sources.

Fourier Transform Spectrometers are built for three reasons; intensity precision and accuracy, high resolving power, and wavenumber accuracy and precision. The throughput advantage and multiplex advantage also make the Fourier Transform Spectroscopy (FTS) attractive but are not the main reasons the worlds most powerful ultraviolet and visible Fourier Transform Spectrometer's have been built.

The first advantage is intensity precision and accuracy in the line profile. This aspect is utilized less than the other two in this research but is used in temperature measurements (e.g. Boltzmann methods involving diatomics (rotational temperature) and atoms (excitation temperature)), line profile studies, isotope ratio determinations, etc. The second advantage is resolution or high resolving power. This advantage was used to look at rotational levels of molecules, physically resolve line profiles, and identify isotope shifts and hyperfine structure of atomic lines. The final advantage

is the excellent wavenumber accuracy and precision. This facet of FT-UV/VIS spectroscopy was utilized to measure line shifts in an Inductively Coupled Plasma (ICP), and better the existing wavenumber accuracy of a well studied N_2^+ transition in ultraviolet. A summation of each chapter follows.

The second chapter is a continuation of my master's thesis. The Helium Inductively Coupled Plasma described in this paper was first developed for nonmetal atomic emission spectroscopy at Los Alamos National Lab (LANL). The source proved to be very stable (low flicker noise component) compared to other flowing systems, had very little background and is sufficiently energetic to be used as a light source. This project was the first published work using the Los Alamos Fourier Transform Spectrometer. It clearly demonstrated that the instrument, a 13 million dollar national facility, was functioning at a high level. It also demonstrated the He-ICP is a good high resolution light source. The $N_2^+(0,0)$ transition was resolved with higher wavenumber accuracy (>1 part in 10^7) than had been previously been reported in the literature.

This same torch was used to generate a low flow, atmospheric pressure Neon Inductively Coupled Plasma. Chapter three is a brief outline of the first Neon Inductively Coupled Plasma described in the literature. This was originally generated for inductively coupled plasma-mass spectrometry studies, but the price of neon proved too expensive to

continue this research.

Chapter four deals with a nonflowing, variable gas inductively coupled plasma as a light source for high resolution spectroscopy. This work was recently issued a patent by the United States Patent office. It generated plasmas with 10 different gases (He, Ne, Ar, Kr, Xe, H_2, N_2, CO_2, C_2H_2, O_2) over a wide range of pressure (0.01-100 torr). Work was also initiated to demonstrate the static, low pressure source could be interfaced to a mass spectrometer with several advantages over the traditional ICP-MS. For Fourier Transform Spectroscopy (FTS) research, the static environment is important to minimize flicker noise in the source. Varying the gas allows us to vary the Doppler temperature and electron density as well as the amount of background light flux.

Chapter five is a physical analytical study. This chapter represents the largest project undertaken; the measurement of line shifts and line profiles of light emitted from a argon inductively coupled plasma. There are small shifts in wavenumber position between low pressure sources (no collisional broadening, no shift) and atmospheric pressure sources. Line profiles were deconvoluted to measure broadening contributions from Doppler and collisional processes in the atmospheric pressure argon ICP. Approximately 180 lines with a signal-to-noise ratio (SNR) greater than 100 were measured with the LAFTS. This pushed

the wavenumber position and resolution capabilities of the FTS technique. Argon, iron, calcium, barium, and strontium emission line profiles from an inductively coupled argon plasma were recorded at sub-Doppler resolution.

The project involving line shifts concluded with the development of a optical filter that allowed variance of both bandpass and wavenumber position. It was designed for ultraviolet and visible Fourier Transform Spectroscopy in conjunction with the ICP. Its purpose was to reduce the amount of unwanted light entering the FTS . This filter is discussed in chapter six.

The Re I (575 nm) line has both hyperfine structure (HFS) and isotope shifts (IS). This structure was proposed as a standard to determine the quality of spectra acquired from a FTS. The reason for doing this is simple. Instrument companies producing instruments have been selling bad instruments, that is Fourier Transform Spectrometers that do not come close to meeting their published specs (often by orders of magnitude). The people purchasing the instruments typically do not know much about FTS and are not aware of the problems. By proposing a standard for wavenumber position, intensity precision, and resolution, it will allow people to judge the quality of the instrument they are about to buy or to judge the performance of the instrument at any given time during its lifetime. It can also serve as a calibration standard when fine tuning the instrument. Chapter seven

describes this standard.

Chapter eight covers noise studies in Fourier Transform Spectroscopy using a relatively simple arrangement. The output of the light source is chopped by a mechanical chopper. Chopping simulates the constructive and destructive interference in an interferometer. When the beam is blocked by the chopper, this simulates destructive interference, and when light is passed, this simulates constructive interference. The beam is chopped at a rate (Hz) similar to that produced by constructive and destructive interference in a Michelson interferometer. This work indicates that a shot noise limited case has not been achieved by analytical spectroscopists, despite their claims.

Analytical spectroscopists typically use a ratio of signal and noise intensities to calculate the signal-to-noise ratio in FTS. This method fails at poor resolutions when the line profile is broadened by instrumental effects decreasing the amplitude (peak height) of the line profile. Provided our integration times are equal, there should be identical signal-to-noise ratios for high and low resolutions alike. This research has found this not to be the case. At poor resolutions, the loss of signal amplitude, caused by instrumental broadening, negatively affects the SNR. Many analytical studies have been carried out at poor resolutions and LODs based on amplitude SNRs giving low values. Many of these studies claim to have achieved shot noise limited cases.

Work in chapter seven gives conclusive evidence that analytical chemists have not achieved a shot noise limited spectra.

CHAPTER 2
USE OF A HIGH RESOLUTION FOURIER TRANSFORM SPECTROMETER TO IDENTIFY THE ROTATIONAL STRUCTURE OF THE $B^2\Sigma_u^+ - X^2\Sigma_g^+$ TRANSITION OF $N_2^+(0,0)$ IN A HELIUM INDUCTIVELY COUPLED PLASMA

Introduction

The use of Fourier Transform Spectrometers in the near, middle and far-infrared spectral region is common in many analytical labs. Since a wealth of atomic information lies in the visible and ultraviolet regions, there has been a great deal of effort by various groups worldwide to build Fourier Transform Spectrometers that operate over this region of the spectrum. In 1975 Horlick and Yuen (1) reviewed spectrochemical analysis with a Fourier Transform Spectrometer (FTS). More recent reviews by Faires (2) and Thorn (3) discuss theory, instrumentation, and applications of a FTS in Atomic Emission Spectroscopy (AES). Stubley and Horlick (4,5,6), Marra and Horlick (7), Faires (8,9), Faires, Palmer, Engleman, and Niemczyk (10), and Faires, Palmer, and Brault (11) carried out pioneering work in FT-ICP-AES. Various aspects of the LAFTS have been previously reported (12,13).

Los Alamos Fourier Transform Spectrometer

The Los Alamos Fourier Transform Spectrometer (LAFTS), housed in a 3360 ft^2 building, is the highest resolution visible and ultraviolet FTS in the world. Table 1 lists some of its characteristics. The instrument is currently operating with single pass optics allowing for a maximum resolution of 0.0026 cm^{-1} (0.023 pm at 300 nm). The interferometer is housed within a 14 foot by 7 foot vacuum tank (30 mTorr achieved) and utilizes two entrance ports for experiments. The FTS sits on a 4 foot by 10 foot NRC vacuum compatible optical table isolating the instrument from vibration.

Figure 1 shows the folded design of the instrument. The LAFTS utilizes a double sided interferogram which improves the signal-to-noise ratio and helps eliminate phase problems. The A/D converter is composed of seven 16-bit A/D converters, scale amplifiers, and an 18-bit D/A converter for calibration. Parsons and Palmer (13) give detailed characteristics and research plans for the LAFTS.

For inductively coupled plasma-atomic emission studies (ICP-AES) the advantages of the FTS are intensity precision, wavenumber accuracy, and high resolution. Provided electronic noise is minimized, the limiting noise in the FT-ICP system will be the plasma. Several papers (14-18) have discussed sources of noise in Argon ICPs.

Helium Inductively Coupled Plasma

Argon is the most common plasma gas used in Inductively Coupled Plasmas for elemental analysis. Abdallah and Mermet (19) compared temperatures of helium and argon in ICP and MIP systems. Abdallah et al. followed with a paper (20) utilizing a 50 MHz Helium-ICP at atmospheric pressure for analytical studies. Seliskar's laboratory (21-24) conducted work with a reduced pressure torch that is adaptable to a commercial ICP unit. Chan et al. (25-27) developed and tested a tangential flow, low flow, atmospheric pressure torch that is constructed entirely of macor and adapts readily to commercial units. Montaser and Van Hoven (28) give a critical review on mixed gas, molecular gas and helium ICPs. Due to the high ionization potential of helium (24.6 eV) versus argon (15.8 eV), it has achieved improved limits of detection for elements with relatively high ionization potentials (Cl 12.9 eV, Br 11.8 eV) (25). He-ICPs have fewer spectral lines than Ar-ICPs in the desired regions of AES decreasing the chance for overlap (26). Tan et al. (29) recently introduced a laminar flow He-ICP torch and demonstrated its use in the analysis of some nonmetals.

$N_2^+(0,0)$

In 1933 Coster and Brons (30) published detailed work on the emission spectrum of N_2^+. Diatomic nitrogen (N_2,N_2^+) has been utilized as a rotational temperature indicator in RF

plasmas (31-39) and various discharges (40-46). Most papers use the unresolved vibrational bandhead or the partially resolved rotational structure. The use of Raman scattering from N_2 as a temperature indicator has also been demonstrated by several groups (47-50). Gottscho et al. (51) give an account of perturbation effects within the $B^2\Sigma u^+ - X^2\Sigma_g^+$ transition of N_2^+. Herzberg (52) gives an excellent discussion of both the theoretical and experimental applications of the transition. Montaser and Van Hoven (28) give references for additional uses of N_2 and N_2^+ in plasma diagnostics. Nitrogen is used in plasmas for metal surface treatment (53), synthesis of nitrogen oxydes (54), and CO, CO_2, and gas lasers (55). The use of N_2^+ in sub-doppler resolution studies is discussed in this paper.

The first negative band of N_2^+ has several advantages for rotational temperature determinations in plasmas. The (0,0) bandhead (391 nm) is in an accessible region of the spectrum. The Q branch ($\Delta J=0$) is forbidden decreasing the number of rotational lines present relative to $N_2(0,0)$, $N_2(0,1)$, and OH(0,0) (56), which are used as rotational temperature indicators. At moderate resolution (<0.25 cm^{-1}), the rotational structure can be adequately resolved.

This chapter presents a low flow, laminar flow, atmospheric pressure helium ICP torch. Nitrogen is seeded into the helium plasma and the emission from N_2^+ is analyzed using the Los Alamos Fourier Transform Spectrometer.

Experimental

Helium inductively coupled plasma torch

The torch is optimized for low flow (2-6 L/min), simplicity in design, and adaptability to a commercial unit. Chan et al. (25) present a low flow (7 L/min), tangential flow, macor torch. Two problems arise with this design. First, macor (Corning, Horseheads, NY), a heat resilient, machinable ceramic, is extremely brittle and time consuming to work with. Second, the spiral design allows the plasma to wrap around the torch at low flow rates increasing the chance for damage to the macor torch. An attempt to run a mixed argon-helium plasma also proved detrimental to the macor. These two problems were overcome by a) reducing the amount of macor and constructing the torch largely from teflon and b) making the torch laminar flow and keeping the plasma above the macor tip.

Figure 2 shows the diagram of the torch used in this study. The plasma gas enters the torch through two side ports spaced 180° apart. Two ports are utilized to give an even distribution of gas through the eight symmetrically spaced channels that carry the plasma gas from the teflon channels through the bores in the macor tip and into the plasma. The sample is carried up through the center of the teflon and macor pieces and enters the plasma region through a 2/1000 inch aperture. The torch handles 10,000 ppm Na solution with no clogging problems. This system uses a fritted disk

nebulizer (11). It has higher efficiency (25% with 0.3 L/min gas flow), lower cost, and a decreased noise power spectrum (14) versus the ultrasonic nebulizer. Helium does not work with a concentric nebulizer due to its relative lack of viscosity versus argon. An extended quartz tube was used to keep impurities (N_2, H_2O etc.) from the atmosphere out of the plasma. It has one or two wraps of teflon tape around its base for an airtight fit with the base. A four turn, gold plated (57) coil was used to generate the 27.12 MHz RF field. The central teflon piece and the teflon base (2" diameter) fit tightly together. The torch is supported on a teflon stand in the ICP box. The tesla coil is attached, via an ignition wire, to one of the side ports with a copper clip. Quartz tubing (1/4" diameter) is inserted into the two side ports. A 12/5 balljoint is inserted into the sample uptake port. The macor tip has a 0.5 inch diameter and a 0.5 inch height. It fits tightly with the teflon channel (see Figure 2). Under normal operating conditions this fit is sufficient to seal the tip from outside contaminants and keep the sample and plasma gas separate. As an added precaution, the outside of the macor-teflon connection is wrapped with teflon tape. The macor to teflon connection can be fused with chemical etching techniques or a high temperature quartz based cement can be used as a sealant. Impedance matching utilized has been previously described in the literature (58,59).

Inductively coupled plasma

This study employs a 27.12 MHz RF Plasma Products (Cherry Hill, NJ) HFP 5000 D model Inductively Coupled Plasma unit. The ICP operating conditions are outlined in table 2. The nitrogen is 99.9995% certified pure and was obtained from Union Carbide-Linde Division (Albuquerque, NM).

Los Alamos Fourier transform spectrometer

The parameters of the LAFTS used for this study are as follows: The spectral output is from 14000 cm^{-1} to 40000 cm^{-1}. The detectors utilized are RCA 1P28s. The beamsplitters are aluminum coated quartz and no optical filters are used. The resolution chosen (0.09 cm^{-1}) is sub-Doppler for nitrogen (19). The number of points taken is 889,219, which is zero filled to 2^{20} (1,048,576) points for transformation. The data acquisition time for the 20 scans is 1 hour 17 minutes and the computer transform time is 42 minutes. The spectrum is unapodized (boxcar). Atmospheric pressure in the LAFTS (7300 ft above sea level) is 593 Torr, and the tank temperature is 21°C.

Results and Discussion

Table 3 gives the line positions (±0.01 cm^{-1}) of the P and R branches observed in the Helium Inductively Coupled Plasma. The accuracy of the (0,0)band data given by Coster and Brons (30) is updated by 0.1 to 0.2 cm^{-1}.

Figure 3 shows part of the (0,0) spectra. The P (1-38)

and R(1-10) branches are identified. The pattern is consistent for larger branch numbers not shown. The doublet splitting (J-1/2,J+1/2) is evident for both branches (P >16, R >10). The alternation of line intensity (even > odd) is unmistakable for both branches. Doublet splitting and even-odd alternation of line intensity are treated theoretically by Herzberg (52).

Figure 4 gives the Fortrat diagram for the P and R branches in the He-ICP. The P branch folds over itself at 25540.10 cm^{-1} giving the vibrational bandhead. The K value used for all branches that are doublet split is J-1/2. At higher K values (R >40, P>44) only the even branches are detectable from this source (He-ICP).

The method to calculate the rotational temperature from a well resolved structure is taken from Abdallah and Mermet (19). This method allows for relative line intensity measurements (as opposed to absolute) for either the P or R branches. For the P branch,

$$\text{Log}\frac{\alpha I}{K''} = f(K''(K''-1)) \qquad (1)$$

and the R branch,

$$\text{Log}\frac{\alpha I}{K''+1} = f((K''+1)(K''+2)) \qquad (2)$$

where α = 1 (even number lines), 2 (odd number lines)
$f = -Bhc/kT = (-2.983/T)$
I = experimental line intensity
K'' = quantum number of lower state
T = temperature (kelvin)

Plotting the left side of equation 1 or 2 (for varying values of I) versus the right side (increasing values of K") of the respective equation yields a straight line with a slope proportional to 1/T. Rotational temperatures for the He-ICP using the parameters and data listed above are R(odd, 1700 K), R(even, 1680 K), P(odd, 1830 K), and P(even, 1660 K).

Various papers (35,38,39) outline similar Boltzmann methods to calculate rotational temperatures in plasmas. This method allows for four rotational temperatures (P (even,odd), R(even,odd)). Thorne (60) claims that the Boltzmann method for $N_2^+(0,0)$ is suitable for measurements under 5000 K. Cabannes (39) claims it is allowable for temperatures under 10000 K. Kornblum and de Galen (61) have interpreted the resulting measurement as the gas kinetic temperature.

Conclusion

A new He-ICP torch has been demonstrated. The torch has also been used to generate a neon ICP (62) and is being investigated as an ionization source for helium and neon ICP-MS studies. The He-ICP is not being pursued for atomic emission spectroscopy.

The use of N_2^+ as a diagnostic tool is common. This paper allows the spectroscopist to easily identify and use the structure for rotational temperatures. The line position accuracy of the rotational levels is improved against those currently in the literature.

Figure 1. Optical Elements: a) cat's-eye reflectors b) beam splitter and carousel c) 8-inch turning mirrors d) collimator optics e) output mirrors . Light enters from either the end or side port and is collimated by d. There it goes to the upper beam splitter, b, and is divided. These two beams go to the turning mirrors c and to the primary mirror of the cat's-eye reflector, a. In the cat's-eye reflector the beam is focused down onto the secondary mirror and reflected back to the primary where it is made parallel again. The effect of the cat's-eye reflector is to reflect the beam back along a path that is parallel but displaced. From the cat's-eye reflectors the beams return to the 8-inch mirrors and then to the lower beam splitter. There the beam is recombined and interferes with itself. The light then travels to the output mirrors, e, that focuses the beam and to the flat mirrors that direct the beam to the detectors.

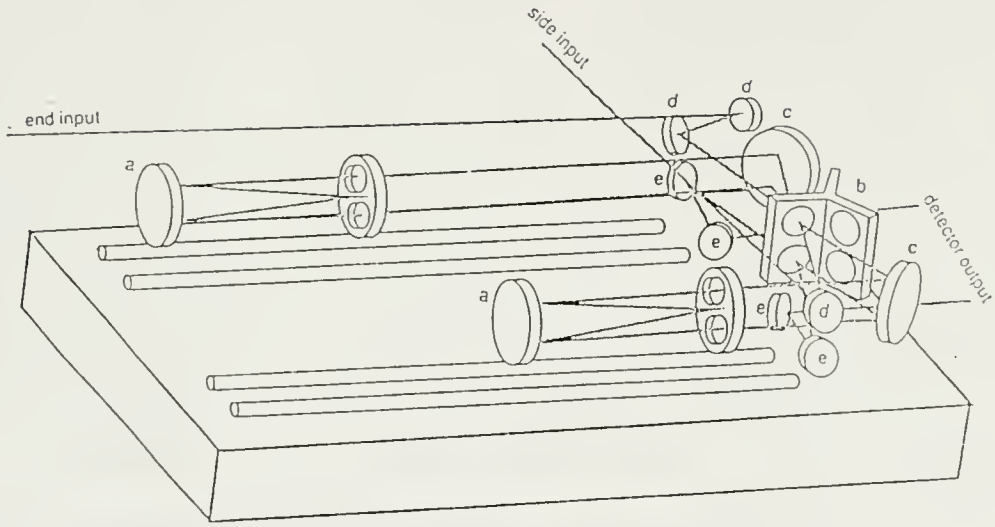
side input
end input
d
d
c
a
e
b
detector output
e
c
a
e
d
e

Figure 2. Diagram of low-flow, atmospheric pressure He-ICP torch. The top inset shows the macor tip and teflon central channel interface in greater detail. The bottom inset shows the eight plasma gas holes surrounding the sample gas inlet on the macor tip.

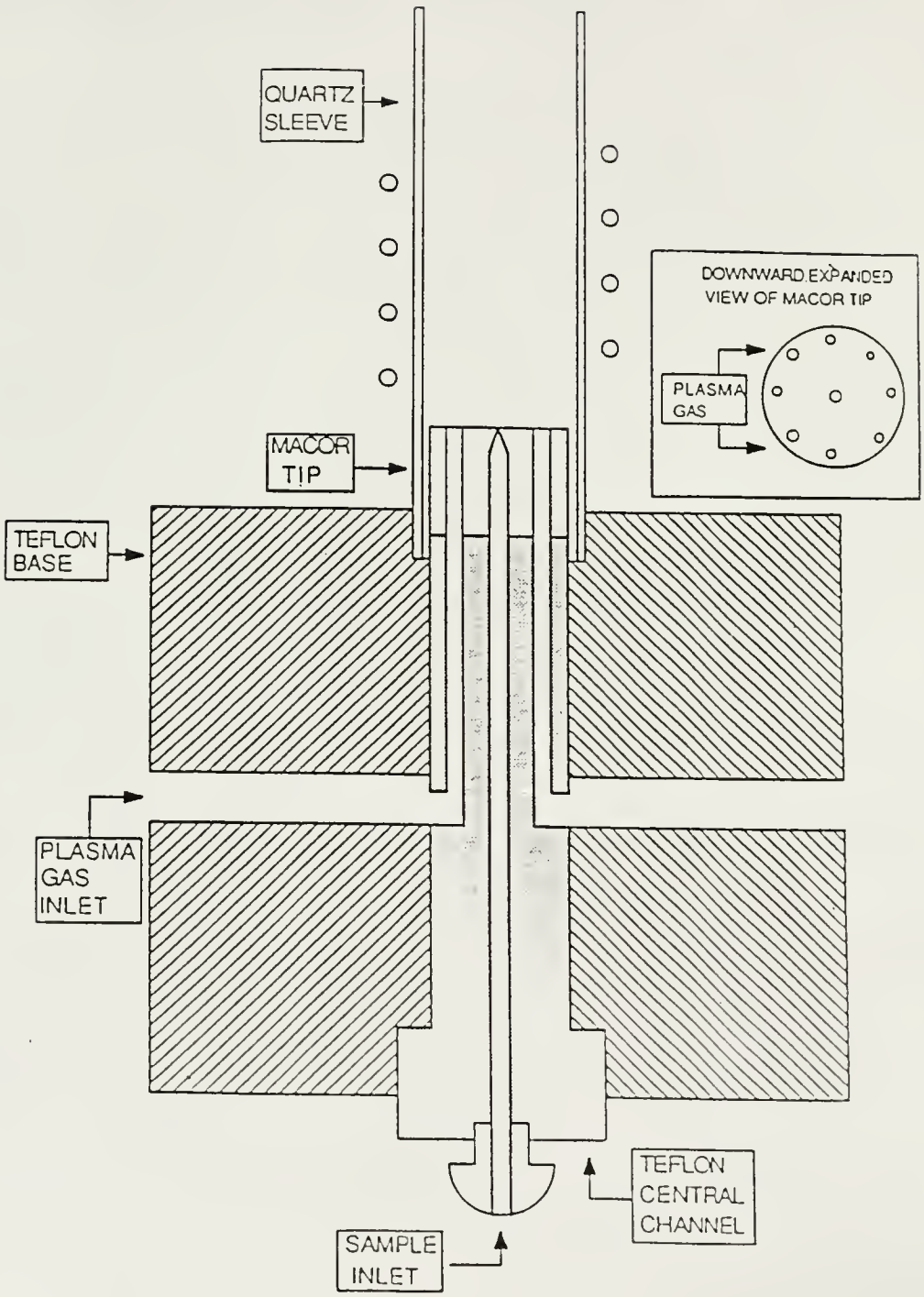
QUARTZ SLEEVE
MACOR TIP
TEFLON BASE
PLASMA GAS INLET
SAMPLE INLET
TEFLON CENTRAL CHANNEL
DOWNWARD EXPANDED VIEW OF MACOR TIP
PLASMA GAS

Figure 3. The four panels show a portion of the rotational structure of the $N_2^+(0,0)$ band. The top x-axis is angstroms and the bottom is wavenumbers (cm^{-1}).

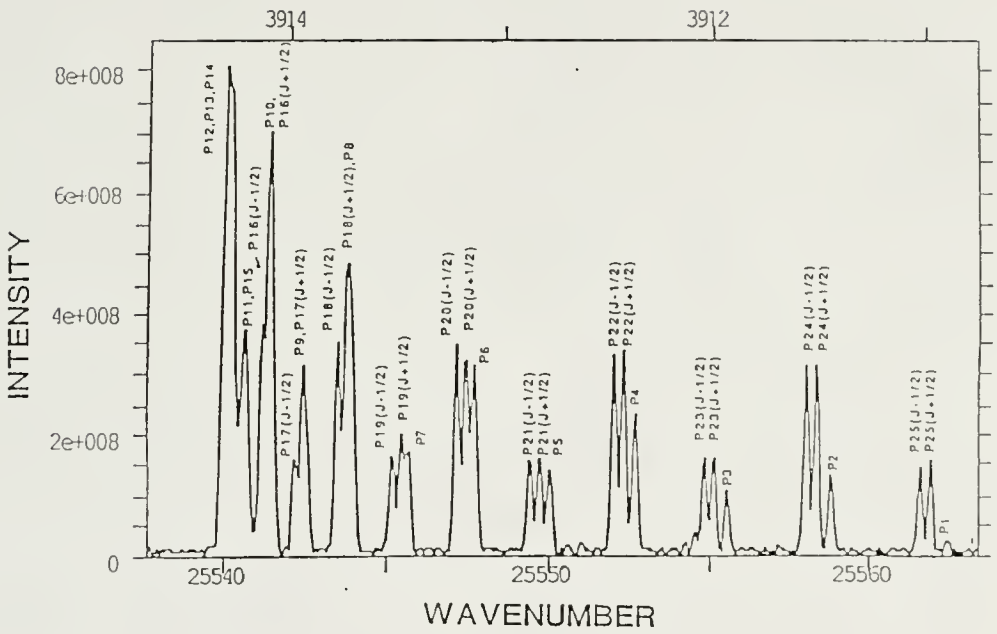
3914
3912
8e+008
6e+008
4e+008
2e+008
0
INTENSITY
25540
25550
25560
WAVENUMBER
P12,P13,P14
P11,P15
P16(J-1/2)
P10,
P16(J+1/2)
P17(J-1/2)
P9,P17(J+1/2)
P18(J-1/2)
P18(J+1/2),P8
P19(J-1/2)
P19(J+1/2)
P7
P20(J-1/2)
P20(J+1/2)
P6
P21(J-1/2)
P21(J+1/2)
P5
P22(J-1/2)
P22(J+1/2)
P4
P23(J-1/2)
P23(J+1/2)
P3
P24(J-1/2)
P24(J+1/2)
P2
P25(J-1/2)
P25(J+1/2)
P1

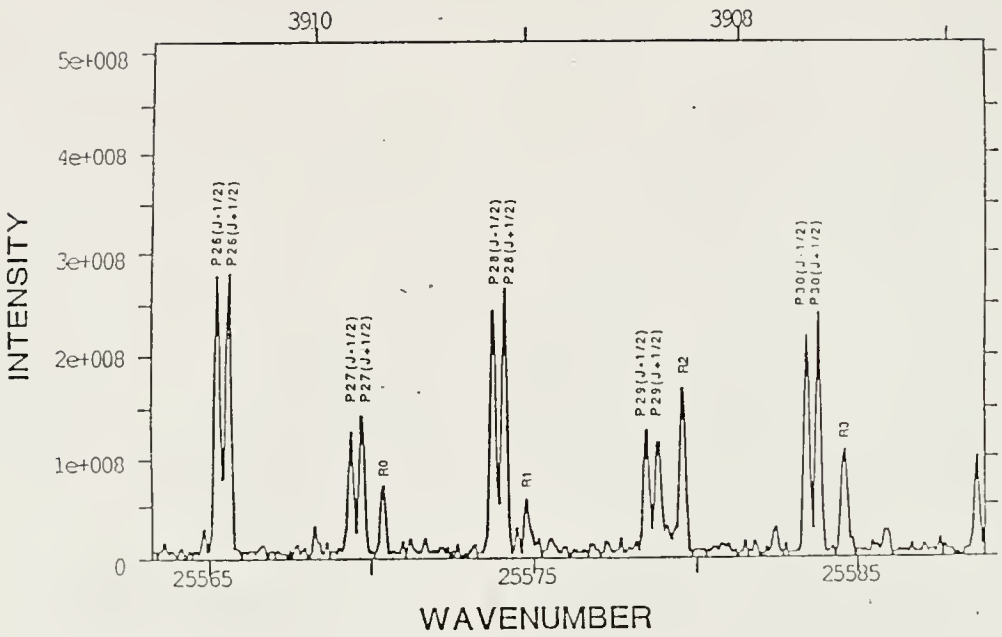

Figure 3--continued

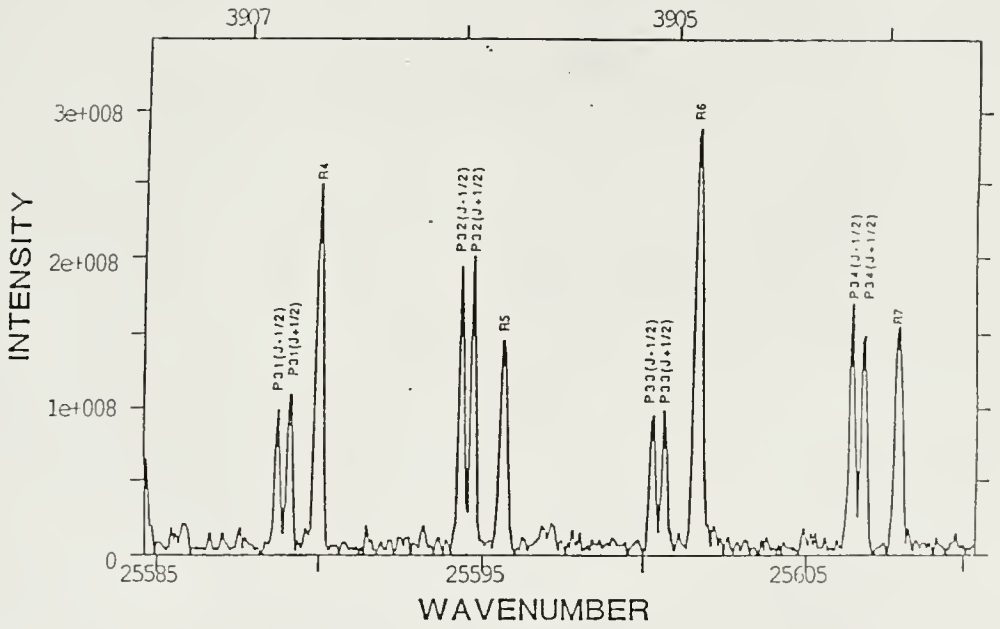

Figure 3--continued

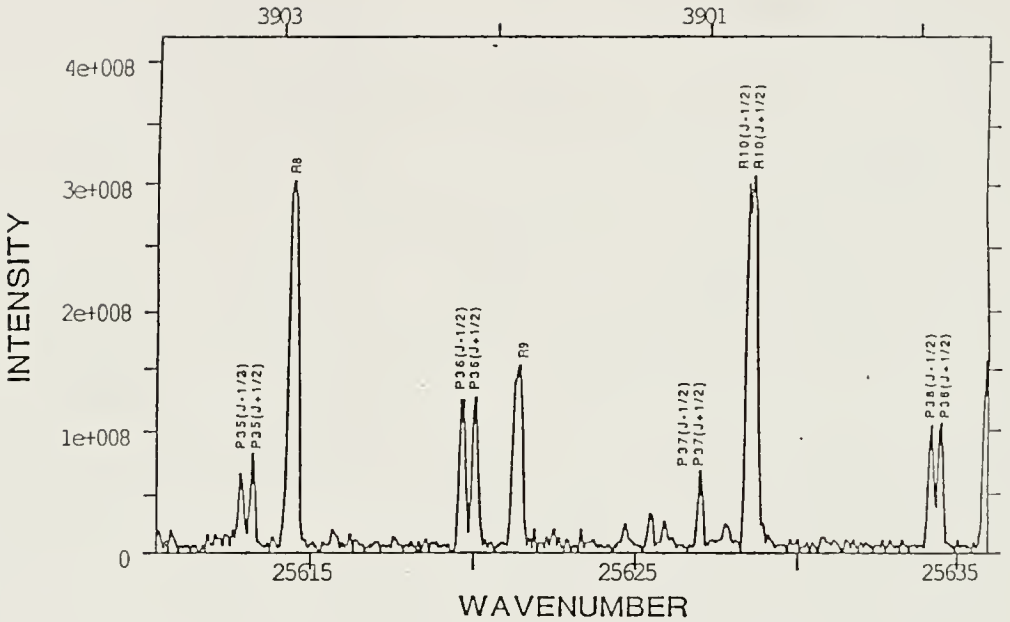

Figure 3--continued

Figure 4. Fortrat diagram of P and R branches. At 25540.10 cm^{-1}, the P branch (P12, P13, P14) folds giving the bandhead.

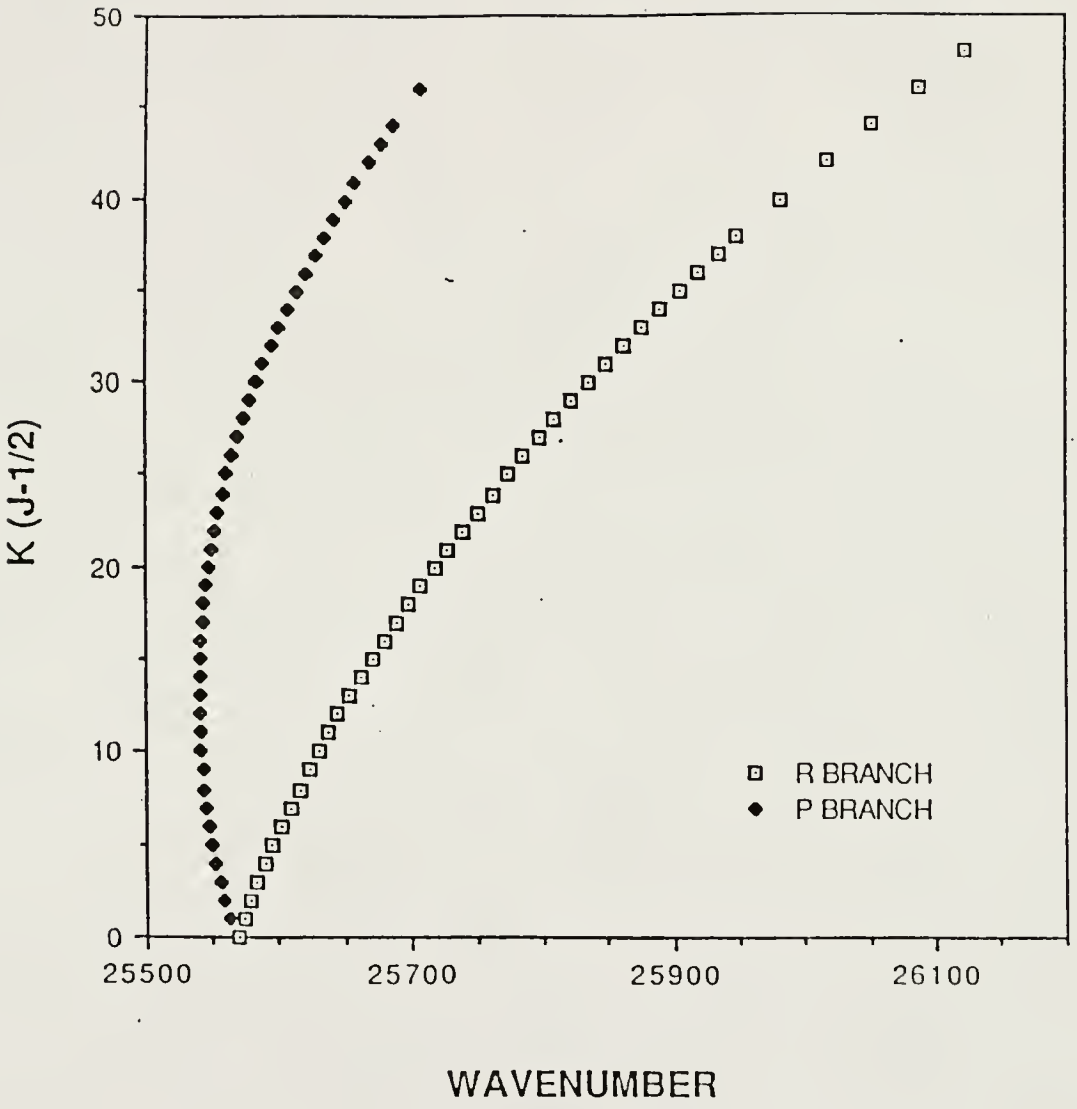
50
40
30
20
10
0
K (J-1/2)
25500
25700
25900
26100
WAVENUMBER
R BRANCH
P BRANCH

Table 1. Los Alamos FOurier Transform Spectrometer Specifications

Spectral Ranges:

Region	Range	Beamsplitters	Detectors
UV/VIS	200 nm-1.1 um	quartz/aluminum	photomultiplier, si PIN diode
NEAR IR	0.8-5.5 um	CaF-GaP	InSb
FAR IR	4-20 um	KCl-Ge	HgCdTe

Resolution and Operating Parameters:

Optical Path Difference	2.5 meters (single pass) 5.0 meters (double pass)
Resolution	0.0026 cm^{-1} (single pass) 0.0013 cm^{-1} (double pass)
Sample Rate	5000 Hz not digitally filtered 40000 Hz with digital filtering reduced to 5000 Hz throughput
Number of points	>4,000,000 points
Maximum Transform Size	2^{22} (4,194,304)

Table 2. Helium inductively coupled plasma operating conditions

Source Unit	RF Plasma-Therm 5 kW unit
Frequency	27.12 MHz
Forward Power	1.5 kW
Reflected Power	<5 W
Plasma Gas Flow	4 L min^{-1}
Nebulizer Flow	0.5 L min^{-1}
Sample Uptake Rate	0.3 mL min^{-1}
Viewing Height above load coil	14 mm
Aperture to FTS	7 mm

Helium inductively coupled plasma.

P BRANCH

K Value	J(±1/2)	WAVENUMBER(cm^{-1})
1		25562.36
2		25558.76
3		25555.54
4		25552.62
5		25549.96
6		25547.66
7		25545.67
8		25543.81
9		25542.47
10		25541.37
11		25540.59
12		25540.11
13		25540.11
14		25540.11
15		25540.59
16	J-1/2	25541.15
16	J+1/2	25541.37
17	J-1/2	25542.16
17	J+1/2	25542.47
18	J-1/2	25543.54
18	J+1/2	25543.85
19	J-1/2	25545.14
19	J+1/2	25545.44
20	J-1/2	25547.12
20	J+1/2	25547.35
21	J-1/2	25549.40
21	J+1/2	25549.65
22	J-1/2	25552.20
22	J+1/2	25552.59
23	J-1/2	25554.82
23	J+1/2	25555.09
24	J-1/2	25557.99
24	J+1/2	25558.28
25	J-1/2	25561.46
25	J+1/2	25561.76
26	J-1/2	25565.24
26	J+1/2	25565.56
27	J-1/2	25569.32
27	J+1/2	25569.66
28	J-1/2	25573.71
28	J+1/2	25574.06
29	J-1/2	25578.42
29	J+1/2	25578.76
30	J-1/2	25583.41

Table 3--continued.

30	J+1/2	25583.77
31	J-1/2	25588.70
31	J+1/2	25589.06
32	J-1/2	25594.31
32	J+1/2	25594.67
33	J-1/2	25600.21
33	J+1/2	25600.56
34	J-1/2	25606.41
34	J+1/2	25606.76
35	J-1/2	25612.88
35	J+1/2	25613.22
36	J-1/2	25619.59
36	J+1/2	25619.99
37	J-1/2	25626.96
37	J+1/2	
38	J-1/2	25634.12
38	J+1/2	25634.39
39	J-1/2	25640.85
39	J+1/2	25641.80
40	J-1/2	25648.44
41		25656.19
42		25668.43
43		25676.62
44		25685.82

R BRANCH

K Value	J(±1/2)	Wavenumber (cm^{-1})
0		25570.30
1		25574.77
2		25579.51
3		25584.57
4		25589.93
5		25595.61
6		25601.58
7		25607.85
8		25614.44
9		25621.33
10	J-1/2	25628.41
10	J+1/2	25628.56
11	J-1/2	25635.89
11	J+1/2	25636.12
12	J-1/2	25643.67
12	J+1/2	25643.90
13	J-1/2	25651.76
13	J+1/2	25651.99
14	J-1/2	25660.16
14	J+1/2	25660.39

Table 3--continued.

15	J-1/2	25668.86
15	J+1/2	25669.09
16	J-1/2	25677.79
16	J+1/2	25678.09
17	J-1/2	25687.18
17	J+1/2	25687.40
18	J-1/2	25696.72
18	J+1/2	25697.02
19	J-1/2	25706.62
19	J+1/2	25706.88
20	J-1/2	25716.78
20	J+1/2	25717.08
21	J-1/2	25727.27
21	J+1/2	25727.58
22	J-1/2	25738.05
22	J+1/2	25738.38
23	J-1/2	25749.15
23	J+1/2	25749.53
24	J-1/2	25760.53
24	J+1/2	25760.86
25	J-1/2	25772.21
25	J+1/2	25772.55
26	J-1/2	25784.17
26	J+1/2	25784.54
27	J-1/2	25796.46
27	J+1/2	25796.82
28	J-1/2	25809.02
28	J+1/2	25809.39
29	J-1/2	25821.89
29	J+1/2	25822.26
30	J-1/2	25835.04
30	J+1/2	25835.41
31	J-1/2	25848.48
31	J+1/2	25848.86
32	J-1/2	25862.21
32	J+1/2	25862.58
33	J-1/2	25876.22
33	J+1/2	25876.59
34	J-1/2	25890.44
34	J+1/2	25890.85
35		25905.36
36	J-1/2	25919.96
36	J+1/2	25920.27
37	J-1/2	25934.16
37	J+1/2	25935.11

CHAPTER 3
GENERATION OF A LOW FLOW ATMOSPHERIC PRESSURE NEON ICP

Introduction

A 27.12 MHz Neon Inductively Coupled Plasma (Ne-ICP) has been generated in this laboratory. Argon has long been used as the plasma gas for an ICP. Abdallah and Mermet (19) and Chan et al.(25) have generated atmospheric pressure helium plasmas in inductively coupled plasma (ICP) units. Walters et al. (63) generated a reduced pressure (0.5-14 torr) 144 MHz neon ICP for electrodeless discharge lamp studies. This is the first known report of an atmospheric Ne-ICP. The torch design has been used for helium ICP studies and is described by Manning et al.(64). The neon ICP is being investigated as a possible atomization source for adaptation to a commercial inductively coupled plasma-mass spectrometry instrument.

Experimental

The Ne-ICP is generated with a 27.12 MHz RF Plasma Products HFP 5 kW unit (Cherry Hill, NJ). The forward power for the ICP is 500 W with less than 5 W reflected (58). The low flow (3 l/min), laminar flow, atmospheric pressure torch is described by Manning et al.(64). It utilizes an extended quartz sleeve to minimize impurities (N_2, H_2O, etc.) from the

atmosphere entering the plasma. The nebulization system employed is the fritted disk nebulizer (11). The sample is pumped to the fritted disk with a standard peristaltic pump. The flow rate of the plasma gas is 3 L/min with a minimum of 2 L/min and a maximum of 7 L/min possible. The nebulizer gas flow rate is 0.3 L/min with a sample uptake rate of 0.3 mL/min. The nitrogen is seeded in at a rate of 5 mL/min. The neon gas is supplied by Union Carbide-Linde division gas distributors (Albuquerque, NM).

Los Alamos Fourier Transform Spectrometer

The Los Alamos Fourier Transform Spectrometer (13), a national facility for high resolution atomic and molecular spectroscopy, is used in this experiment for medium resolution (0.07 cm^{-1}) spectra in the near IR, visible, and ultraviolet (8500 cm^{-1} to 33372 cm^{-1}). Aluminum coated quartz beamsplitters are employed and the detectors utilized are silicon PIN diodes. The number of points taken for each run is 953,863 and the transform size is 2^{20} (1046000) points. The run in which only water is introduced into the plasma consists of 10 scans (39 minutes data acquisition time) and took 16 scans in the run introducing both water and N_2 (64 minutes data acquisition time). The number of scans is limited by the current availability of research grade neon. The cost of neon is the limiting factor.

Results and Discussion

Neons' ionization potential (21.56 eV) is higher than that of argon (15.76 eV) but lower than helium (24.587 eV). This should offer better detection limits for various nonmetals (eg. F, Cl, Br, etc.). The neon plasma as a source does not have the luminosity of the argon ICP and is similar to the helium ICP in this respect. The plasma is stable with powers as high as 1.5 kW. Introducing sample reduces its stability. With an aerosol entering the plasma, it could not operate at powers greater than 600 W. Above this threshold the plasma either extinguished or formed numerous filaments and produced a non-homogeneous plasma. The plasma operated with powers as low as 150 W. Luminosity appears linear with power.

An attempt to measure the rotational temperature using N_2^+(0,0) (391.44 nm) and OH(0,0) (306.4 nm) is made. The N_2^+ bandhead has a SNR of 4.2 and the R branches used in diagnostics are not discernible making reliable measurements impossible. The OH(0,0) band is not present at all in the spectrum. The H_β line is used to measure the electron number density (65) at 8×10^{13} cm^{-3}. The fact that both species (OH, N_2^+), which are strong UV emitters in plasmas and discharges, do not have a readily detectable emission rate, coupled with the low electron density measurement (8×10^{13} cm^{-3}) and the low input power (500 W), give reason to believe the Ne-ICP in this setup is cool compared to the argon and helium

plasmas (19) run at higher powers. Bands from the first positive system ($B^3\Sigma_g$ - $A^{3\Pi}{}_u$) of N_2 are obvious in the near IR and visible. This transition (10,000 cm^{-1}-17,000 cm^{-1}) requires less energy for excitation than OH(0,0) (>31,000 cm^{-1}).

Conclusion

An atmospheric pressure neon ICP is generated. In the current setup it operates reliably at 500 W forward power. The Ne-ICP is being pursued as an atomization source for a commercial ICP-MS setup. A greater amount of diagnostics is not feasible due to the expense of running a Ne-ICP. A single Ne line (585 nm) was used to determine the Doppler temperature. The value (1058 K) was obtained by deconvoluting the line profile with a Voigt profile.

Using a Ne-ICP as an ion source for ICP-MS studies should offer the advantage of "freeing" various mass values that are not accessible with argon as the plasma gas.

CHAPTER 4
A NON-FLOWING, VARIABLE GAS INDUCTIVELY COUPLED PLASMA AS A LIGHT SOURCE FOR HIGH RESOLUTION SPECTROSCOPY

Introduction

Ten self-contained 27.12 MHz Inductively Coupled Plasmas (ICP) are generated in a static torch. The torch offers spectroscopists a closed system, low pressure (0.01 to 100 Torr), variable power (currently up to 1 kW) plasma. Doppler temperatures (Na D, 589.0 nm) measured are approximately 5 times that of electrodeless discharge lamps (EDLs) or Hollow Cathode Lamps (HCLs) operating under normal conditions. It has improved noise considerations verses the flowing ICP traditionally used.

Plasmas are generated using helium, neon, argon, xenon, krypton, hydrogen, nitrogen, oxygen, carbon dioxide, and ethylene. In some cases, particularly xenon, the closed system minimizes the consumption of expensive gases. In the case of hydrogen, it minimizes the potential hazard of working with the gas in a flowing system. Ideas for absorption, ICP-MS, and lasing action in a static plasma are discussed. This torch generates a low noise, high power plasma that can be used for a variety of spectroscopic studies.

Experimental

Figure 5 shows the torch design utilized in this study. The quartz tube has a 17 mm OD, 15 mm ID, and a 14 cm length. A quartz window is fused to the viewing end of the tube. In some circumstances, using grounded clips helps the plasma symmetrically fill the entire tube. End on viewing increases the luminosity of the source. The four turn coil is gold plated 1/8 inch copper tubing. The ICP instrument is a RF Plasma Products HFP 5000 D (5 kW) unit. Often the plasmas are initiated by introducing the field (RF ON) and slowly increasing the power. In instances where this is not possible (typically >10 Torr), a tesla coil discharge is sent through one of the grounded clips to ignite the plasma. A vacuum rack equipped with a liquid nitrogen cold finger, a roughing pump, and a diffusion pump is utilized for evacuating the cell and filling it with the desired gas. The cell is evacuated to 10^{-5} Torr, back filled with the desired plasma gas, evacuated to 10^{-5} Torr, and filled to the desired pressure.

The cell is demountable and easily inserted into the ICP coil. A 12/5 balljoint connects the rack and the torch. As a precaution, nitrogen is blown across the quartz torch for cooling purposes. Pressures given are the fill values at room temperature. Powers recorded are the forward minus the reflected values.

The Los Alamos Fourier Transform Spectrometer is used to

record the spectra at high (0.039 cm^{-1}) resolution with 5 scans. The detectors are Silicon PIN diodes, and the beamsplitters are aluminum coated quartz. The spectral window transformed is from 8500 cm^{-1} to 40000 cm^{-1}. 2,052,056 points are acquired and zero filled to 2,097,152 (2^{21}) points. Additional parameters of the LAFTS are supplied by Manning et al (64) and Parsons and Palmer (13). All gases used are certified research grade (>99.995 %).

Results

Figure 6 shows the Na D (589.0 nm) line profile in a Xe-ICP. Sodium (and lithium) impurities are present in most of the spectra obtained. They are attributed to impurities in the quartz. The sodium D line is used for the determination of the Doppler temperatures in each plasma. Values ranged from xenon (7 torr, 250 W) at 3700 K to both carbon dioxide (2.8 torr, 250 W) and oxygen (6 torr, 550 W) at 2400 K. These values are approximately 5 times that of HCLs or microwave-EDLs, assuming a normal current or power input. To avoid having the sample absorb on the cooler ends of the torch, the length of the torch may have to be reduced so the tube length fits entirely within the coil. Adding small quantities of a desired species (e.g., typically in the 1-10 microgram range) allows the torch to be used as a stable reservoir of atomic lines. The same is possible for molecules stable in the plasma environment.

The low pressure inert gas (He, Ne, Ar, Kr, Xe) plasmas seeded with trace amounts of N_2 for diagnostic measurements exhibited varying degrees of continuum emission in the near IR and visible. Xenon is the most prevalent with approximately 15 prominent continuum emission bands. The signal to background measurements of the emission bands ranged from 3 to 15 and are typically 2-3 nanometers wide. The bands are found between 625 and 880 nm. They are semicircular in appearance.

Discussion

The analysis of atomic and molecular species stable in a static plasma utilizes some of the capabilities of the UV/Vis Fourier transform spectrometer (particularly the LAFTS). In particular the intensity precision, wavenumber position precision and accuracy, and resolution capabilities are partially realized.

There is no reason to believe this cell could not generate other plasmas. Atomic species which are gaseous at low pressure (mercury, radon, volatile salts), diatomic gases (NO, CO, Cl_2, Fl_2, etc.), polyatomic gases (NO_2, SO_2, C_2H_2, other hydrocarbons, etc.) should readily form low pressure plasmas in this setup. The ethylene-ICP and other hydrocarbons systems may be of interest to those studying the diamond synthesis mechanism in a RF-plasma environment (66). Closed cell hydrogen-ICP minimizes the dangers of working with a flowing system. This hydrogen-ICP allows scientists to study

atomic interactions in a system similar to the surface of cooler stars.

Fusing quartz windows to both ends of the plasma tube allows a variety of absorption measurements to be conceived. For example, intracavity absorption (67) with an ICP is possible with the advantage of a longer path length, smaller sample size, and an increased residence time per atom verses the traditional flowing ICP torch.

A closed system ICP is currently being investigated as an ion source for mass spectrometry. One end of the tube is directly interfaced to the mass spectrometer with the flow regulated by a gated valve. The sample is injected through the syringe port (0.1 to 1 microliter) before ignition. The solvent evaporation is enhanced with the vacuum leaving only sample in the quartz tube. With plasma ignition, the sample sputters into the plasma. We have found this to work quite well for the nonmetals and softer metals. The variable gas static plasma for ICP-MS should offer many advantages over the flowing argon system. Expensive gases (e.g., neon, krypton, xenon) can be routinely used due to low gas consumption. These inert gases may be used to free mass ranges not accessible with argon (e.g., sample overlaps with ArN^+, ArH^+, $ArOH^+$, etc.). Provided experimental conditions are identical (power, pressure), the temperature and electron density of the inert gas plasma (He, Ne, Ar, Kr, Xe) will have an inverse relationship with the ionization potential. That is, the

higher the ionization potential is, the lower the temperature and electron density will be. Thus by varying the inert gas, the temperature and electron density range can be varied. The closed cell allows for small sample sizes. It reduces some of the hazards associated with radioactive samples in a flowing system. The pressure differential between the plasma and the mass spectrometer is reduced by at least two orders of magnitude. Problems associated with the skimmer/orifice degradation are reduced. The sample waste associated with a flowing system is minimized. Nebulization is eliminated. In some situations it may be possible to use nonpolar samples and solvents. With evaporation/dehydration techniques, the formation of hydrides, hydroxides, and oxides will hopefully be reduced by applying this procedure. The low pressure cell operated here can be converted to a fireball (68) at higher powers. The fireball resembles the atmospheric pressure argon ICP in appearance. This fireball could not be sustained for extended periods of time or the quartz would glow red and eventually melt. If a continuous vacuum is applied that maintains a constant pressure, the fireball can be maintained for extended periods of time.

Eckert (69) gives an excellent theoretical discussion of elemental detection in a static induction plasma. His calculations predict a limit of detection for magnesium (279.6 nm line) of less than 10^{-15} g in a nonflowing argon-ICP. With small modifications to the torch, the closed cell ICP may have

analytical usefulness. This analytical research would be similiar to work previously carried out with microwave electrodeless discharge lamps.

Conclusion

The static plasma outlined in this note describes an atom and molecule reservoir for spectroscopic studies (70). It is also being pursued as an ion source for mass spectrometry (70). No graphical data is presented to support the claim that noise factors in the static plasma are improved over the flowing system. We hope the reader follows the reasoning that with the lack of turbulence induced by the gas flow, and no nebulization system, many of the sources of noise inherent in a flowing system are either reduced or eliminated in a static plasma. The intensity variation as a function of time is at least an order of magnitude improvement over the flowing system under normal operating conditions.

With various adaptations to the cavity, the cell could be used for a variety of emission, absorbance, and fluorescence measurements, both analytical and physical in nature.

Figure 5. Closed cell ICP torch design.

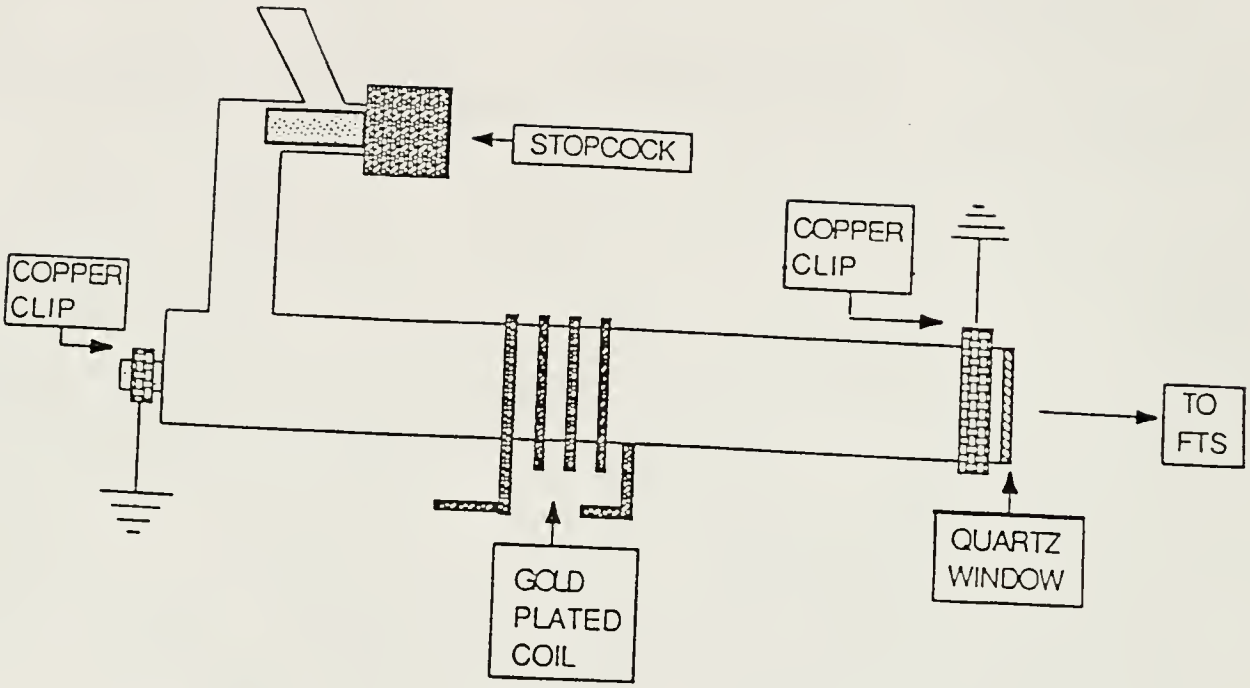
STOPCOCK
COPPER CLIP
COPPER CLIP
TO FTS
GOLD PLATED COIL
QUARTZ WINDOW

Figure 6. Line profile of Sodium-D (589.0 nm) in Xe-ICP.

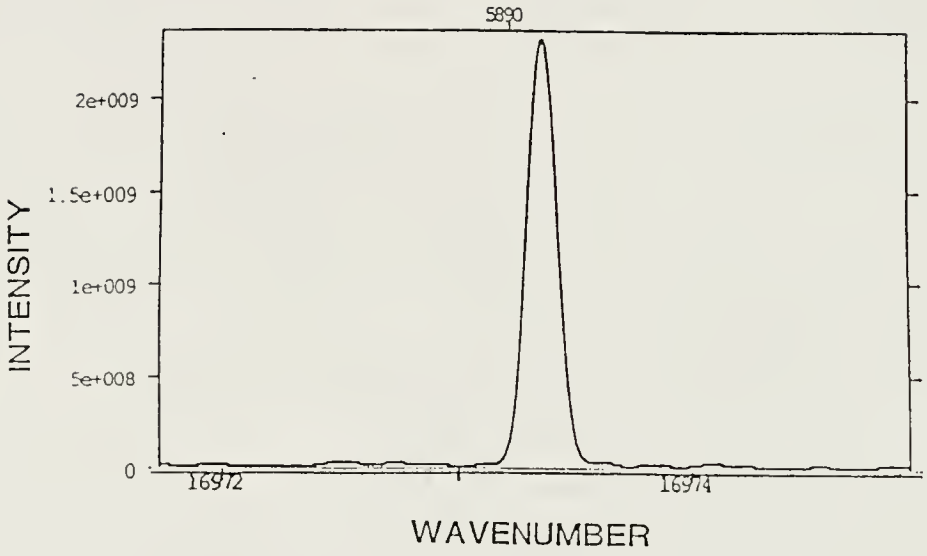
5890
2e+009
1.5e+009
1e+009
5e+008
0
INTENSITY
16972
16974
WAVENUMBER

CHAPTER 5
OBSERVATION OF LINE SHIFTS AND LINE PROFILES IN AN INDUCTIVELY COUPLED ARGON PLASMA

Introduction

Line shifts in analytical inductively coupled plasma's (ICP) are a fundamental parameter that has not been studied in any great detail. This paper will give an introduction to line shifts measured and trends observed. For more detailed treatments of pressure effects, including line shifts, the reader is directed to Thorn (60) (overview), Alkemade et al. (71) (in flames), Griem (72), and Breene (73) and references within. Reviews by Konjevic and Weise (74) and by Konjevic and Roberts (75) give numerous references on Stark broadening and line shifts from a variety of sources.

Line shifts are important for a variety of reasons. Analytical determination of elements in a complex sample is often plagued misidentification of the species being studied. In physical spectroscopy, ICPs are being used for the measurement of transition probabilities. Knowledge of line shift values are important to properly measure energy levels, transitions, etc.. Whaling and Brault (76) used an ICP in conjunction with the Kitt Peak Fourier Transform Spectrometer to measure the transition probabilities of 1200 Mo (I) lines;

they introduce Mo as $Mo(CO)_6$ eliminating any effects water has on the spectrum. They observed line shifts of Mo as great as 0.14 cm^{-1}.

The Los Alamos Fourier Transform Spectrometer (LAFTS) is an ideal instrument to measure small spectral shifts. Its high resolution capabilities easily resolve physical line widths emitted by hollow cathode lamps (HCL) (0.025 cm^{-1}) and the inductively coupled plasma, (0.07 cm^{-1}). The wavenumber precision of the LAFTS can be as great as 1 part in 10^8. The LAFTS can acquire large spectral windows (9000 to 42000 cm^{-1}) at the required resolution to physically resolve the ICP emission.

In studying line shifts, isotope shifts and hyperfine structure must be considered to properly select a line. Elements that clearly display either effect are avoided due to the complexity introduced in attempting line profile studies. The spectrum of a Pb emission line shows contributions from three isotopes, $_{82}Pb^{206}$ (24.1%), $_{82}Pb^{207}$ (22.1%), and $_{82}Pb^{208}$ (52.4%). These isotope shifts are shown in Fig. 7. This spectrum was taken from a low pressure HCL with a Doppler temperature of approximately 500 K, resulting in Doppler broadened spectral lines having negligible pressure (collisional) broadening. Increasing the temperature to 6500 K and introducing substantial amounts of collisional broadening, which simulates ICP conditions, will cause the three isotopic lines to appear as one asymmetric, broadened line. Measuring the line shift

becomes difficult because the individual lines have to be deconvoluted before spectral shift measurements are possible. There will be uncertainty introduced into the calculation by the deconvolution which may affect the validity of the shift measurement.

Figure 8 shows the hyperfine structure of tantalum. $_{73}Ta^{181}$ is the predominant isotope occurring naturally (99.998%) so isotopic effects are negligible. With a nuclear spin of 7/2, $_{73}Ta^{181}$ clearly exhibits hyperfine structure. Kuhn (77) gives an excellent treatment of hyperfine structure and isotope shifts. Ta emission in an ICP has significant Doppler and pressure broadening of the lines giving asymmetric line profiles with 8 convoluted hyperfine elements making shift measurements virtually impossible.

Argon has one predominant isotope ($_{18}Ar^{40}$,99.60%) which has no nuclear spin making it an ideal choice for line shift studies. Figure 9 shows a line profile typical of Ar I emission at 420 nm from the ICP. Iron has one dominant isotope ($_{26}Fe^{56}$, 91.72%), which has no hyperfine structure; Fig. 10 shows a line profile of Fe I at 259.9 nm. The effect of the lower abundance isotopes of Fe on the line center position (shift measurement) and the full width at half maximum (FWHM, $\underline{a}$-parameters; where $\underline{a} = 0.86*(\lambda_L/\lambda_D)$ are considered negligible for this study.

Kato et al. (78) measured profiles of 16 spectral lines stemming from 8 elements emitted by an ICP and measured with

a pressure-scanning Fabry-Perot interferometer. The results their study are similar in absolute magnitude of some lines but occasionally differ in sign. They did not consider the effects of hyperfine structure and/or isotope shifts as carefully as we did. Boumans and Vrakking (79) published work on high-resolution spectroscopy using an echelle spectrometer, which refers to line shifts in the ICP in connection with the wavelength calibration of the spectrometer.

Experimental

The Los Alamos Fourier Transform Spectrometer (LAFTS) is utilized in conjunction with a 27.12 MHz RF Plasma Therm (Cherry Hill, NJ) ICP. Papers by Manning et al. (64) and Parsons and Palmer (13) give details of the LAFTS. For all studies, the viewing height above the coils is 12 mm. The gas flow rates are 12 L/min (outer), 0.8 L/min (intermediate), and 0.8 L/min (nebulizer). For ICP studies, the LAFTS was operated at 0.07 cm^{-1} resolution with a free spectral range of 33005.2 cm^{-1}. For the HCL studies, the LAFTS was operated at 0.02 cm^{-1} resolution with a free spectral range of 40015.2 cm^{-1}. The detectors used were PMTs (1P28) or silicon pin diodes. The silicon pin diodes were utilized for work involving Ar emission in the near IR.

The output of the light source (ICP or HCL) is focused with unity magnification on the FTS spectrometer aperture. The f number of this spectrometer and the ICP/HCL optical

setups are matched. The output of a neon filled Al HCL is impressed on the ICP emission using a neutral density filter (0.2) before the focusing optics. Figure 11 shows an outline of the entrance optics and the light sources. The Ne I line at 585.2 nm from the HCL is used as a calibration standard for all runs.

All emission lines used in this study (HCL and ICP) have signal to noise ratios (SNR) greater than 100. This requirement reduced the number of lines available between the two sources. Some strong lines in the HCL were not always as prevalent in the ICP and vice versa. Ionic lines for iron and argon detected in the ICP were not observed in HCL emission or had low signal-to-noise ratios, reducing the accuracy and precision of the wavenumber measurement.

Six {Fe (1.1, 1.5, 1.9 kW), Ar (1.1, 1.5, 1.9 Kw)} Doppler temperatures were calculated from the ICP emission line profiles using a Voigt fit. This Doppler temperature was then used for all calculations involving those particular conditions. For example, an Fe I line with a high SNR is chosen from the 1.1 Kw ICP data. Voigt profiles are generated until one is identical to the Fe I (ICP) profile. This allowed us to estimate the contributions from Gaussian (Doppler broadening) and Lorenztian (collisional broadening) components. The Gaussian component is then used for all line profile calculations involving Fe emission from the ICP at 1.1 kW. We measured the Gaussian and Lorentzian contributions for

one Ar and one Fe spectral line at each power level (1.1, 1.5, 1.9 kW) giving a total of six Doppler temperatures.

The H_β line is used to estimate the electron density in the analytical zone viewed by the LAFTS. These electron densities applied only to the analytical zone; the region where the Fe, Ba, Ca, and Sr emission predominantly occurs is studied. Ar emission is not predominantly from the analytical zone but from the outer tangential flow zone. No electron density calculations were made for the latter zone.

Results and Discussion

The results are separated into three groups. First, Fe and Ar emission lines in the ultraviolet and visible at three separate power settings (1.1, 1.5, 1.9 kW) were measured. Second, Ar emission in the near infrared and far visible was measured. Third, prominent ion lines of Ca, Sr, and Ba at 1.1 kW were measured.

The first section refers to line shifts as a function of power for 28 Fe lines and 21 Ar lines in the ICP. The power dependence (1.1, 1.5, 1.9 Kw) is shown to increase Doppler temperature, electron density, and shift. The iron data are refer to the analytical zone of the ICP, whereas the argon data refers to the outer tangential flow. For the argon and iron data, the line position is given in Angstroms and physical parameters (line shift, width, etc.) are given in wavenumbers (cm^{-1}). Line positions are given in Angstroms

because the references used for transition assignments list them in this manner. Most research measuring line shifts report their results in cm^{-1}.

Table 4 gives the Doppler temperature (6500 K), transitions types, wavelengths, line shifts, Doppler and Lorentzian contributions to the line profile, and the a-parameter for 21 argon lines at 1.1 Kw. Transition assignments for the Ar-term configurations are taken from Li and Humphrey (80). A single argon line at this power is fitted with a Voigt profile to approximate the Doppler contribution to the line profile. The resulting Doppler temperature of 6500 K is then used to calculate the Doppler half-width and a-parameter for all argon lines at this power and the Lorenztian contribution is calculated with an iterative method:

$$\Delta\nu_V = (1/2)*\Delta\nu_L + \sqrt{((1/4)*\Delta\nu_L^2 + \Delta\nu_D^2)} \quad (3)$$

where $\Delta\nu_v$ is the total line width, $\Delta\nu_L$ is the Lorentzian component, and $\Delta\nu_D$ is the Doppler component.

All line shift values given are shifted towards the red(positive values). Negative values are blue shift. Tables 5 and 6 give similar data for Ar at 1.5 and 1.9 kW respectively.

Figure 12 shows the relationship between <r>, the average distance of the electron from the nucleus and the average shift for the 6p-4s, 5p-4s, and 4p-4s transitions of argon at

each of the three powers. The <r> values for 6p, 5p, and 4p levels are estimated using

$$<r> = (1/2)a_o[3n^2 - l(l+1)] \qquad (4)$$

where a_o is the Bohr radius, n is principle quantum number, and l is the azimuthal quantum number.

In Tables 7,8, and 9, give the results for Fe at 1.1, 1.5, and 1.9 kW, respectively. For each table (power level), a Doppler temperature and electron density are calculated. The electron density was calculated using the H_β line (486.1 nm). The transition configuration, wavelength of transition, line shift, FWHM, Doppler and Lorentzian contributions to the line profile, and the a-parameter for each line profile studied have been measured. The iron concentration was 1000 μg/ml for all runs. The Fe transition assignments were taken from Fuhr, Martin, and Wiese (81).

In Table 10, the spectral characteristics of 25 additional argon lines obtained with the ICP (1.1 Kw) in the near-IR and far visible are also given. A large number of intense Ar lines emitted from the ICP and the HCL occur in this region. It contains exclusively 4p-4s transitions.

In Table 11, the final set of data presents line shifts of calcium, barium, and strontium in a 1.1 Kw ICP are given. These lines are used to investigate the relevance of line shifts in analytical spectroscopy. We consider each element

to have minimal isotope effects ($_{20}Ca^{40}$ (96.97%), $_{38}Sr^{88}$ (82.56%), $_{56}Ba^{138}$ (71.66%)); there are no hyperfine structures on the major isotopes. The electron density and Doppler temperature are considered to be the same as those in table 4 (Fe at 1.1 kW). Emission from these ions are typically blue shifted.

Conclusion

The purpose of this chapter is to report the results of measurements of shifts in line positions that are a function of pressure broadening, in particular, Stark broadening. Fe shows red shifts are on the order of 0.01-0.03 cm^{-1}. Line shift studies on Ca, Sr, and Ba resulted in shifts of the same absolute value as those of Fe but containing a number of blue shifts. Line shifts for Ar in the visible and ultraviolet are equivalent to or greater than those for those for Fe. The shifts for 6p-4s transition is largest, followed by the 5p-4s transitions and the 4p-4s transitions. We also show that line shifts for Ar increase with power. Line shifts are shown to increase as the average distance of the electron from the nucleus radius increases provided the lower (ground) state is the same for all three transitions.

From our measurements, line shifts should have little consequence to the analytical spectroscopist. The data from Ca, Ba, Sr, and Fe shows that the average shift is on the order of 0.01-0.03 cm^{-1}. Line positions of this accuracy are not readily measurable by most analytical systems.

Figure 7. Only one of Pb's three isotopes has any hyperfine structure ($_{82}Pb^{207}$). In the ICP, this isotope structure would be convoluted into one asymmetric line profile making line shift measurements of each line extremely difficult. (Top x-axis is Å and the bottom is in wavenumbers, cm^{-1}).

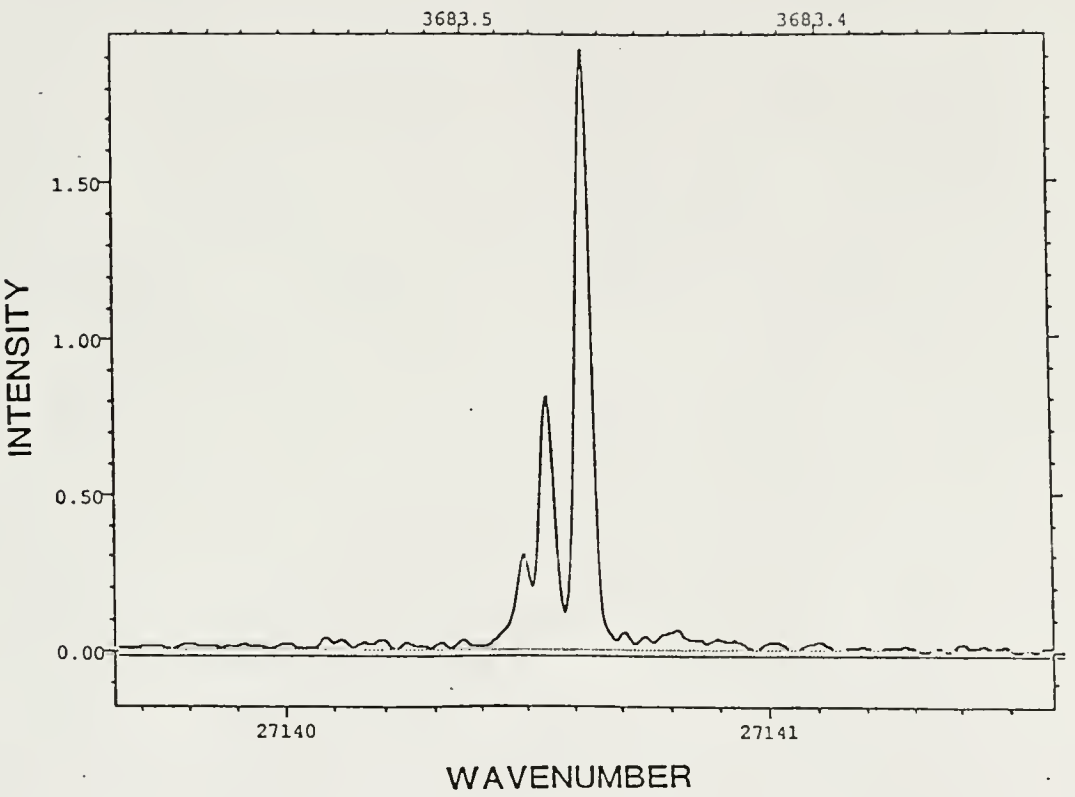
3683.5
3683.4
1.50
1.00
0.50
0.00
INTENSITY
27140
27141
WAVENUMBER

Figure 8. The hyperfine structure of $_{73}Ta^{181}$ taken from a low pressure HCL. The higher pressure and temperature of the ICP would make line selection difficult. (top x-axis is Å and the bottom is cm^{-1})

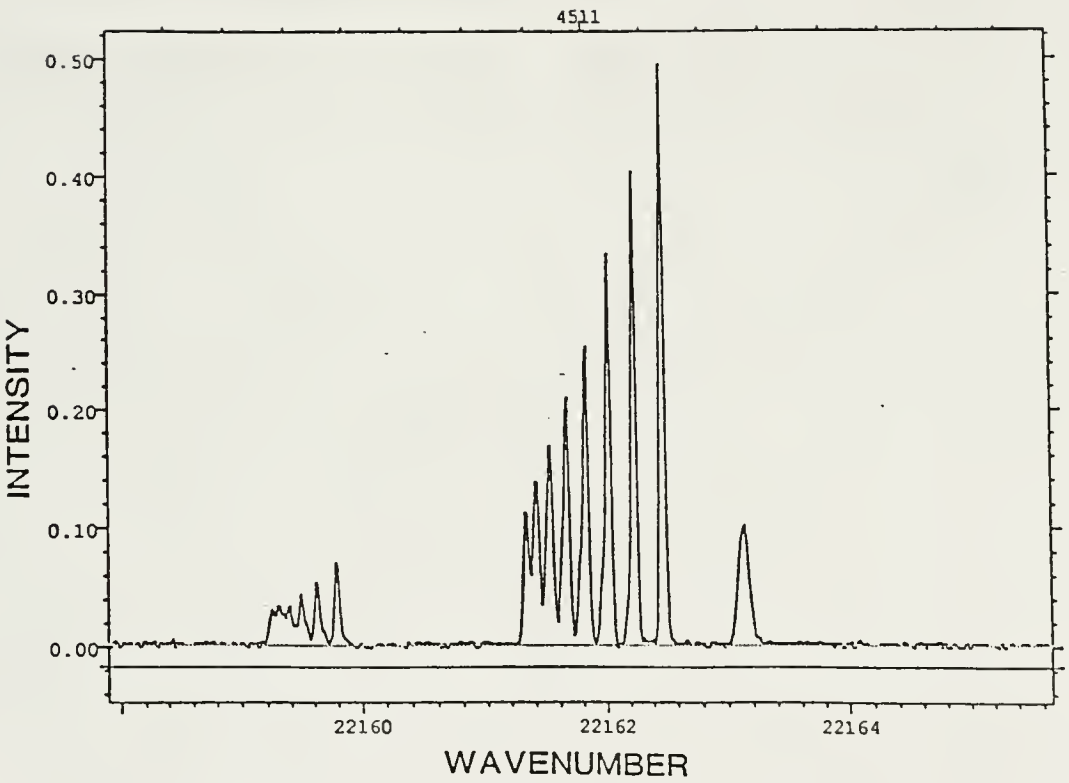
4511
0.50
0.40
0.30
0.20
0.10
0.00
INTENSITY
22160
22162
22164
WAVENUMBER

Figure 9. Typical line profile of Ar I emission from the ICP. (top x-axis is Å and the bottom is cm^{-1})

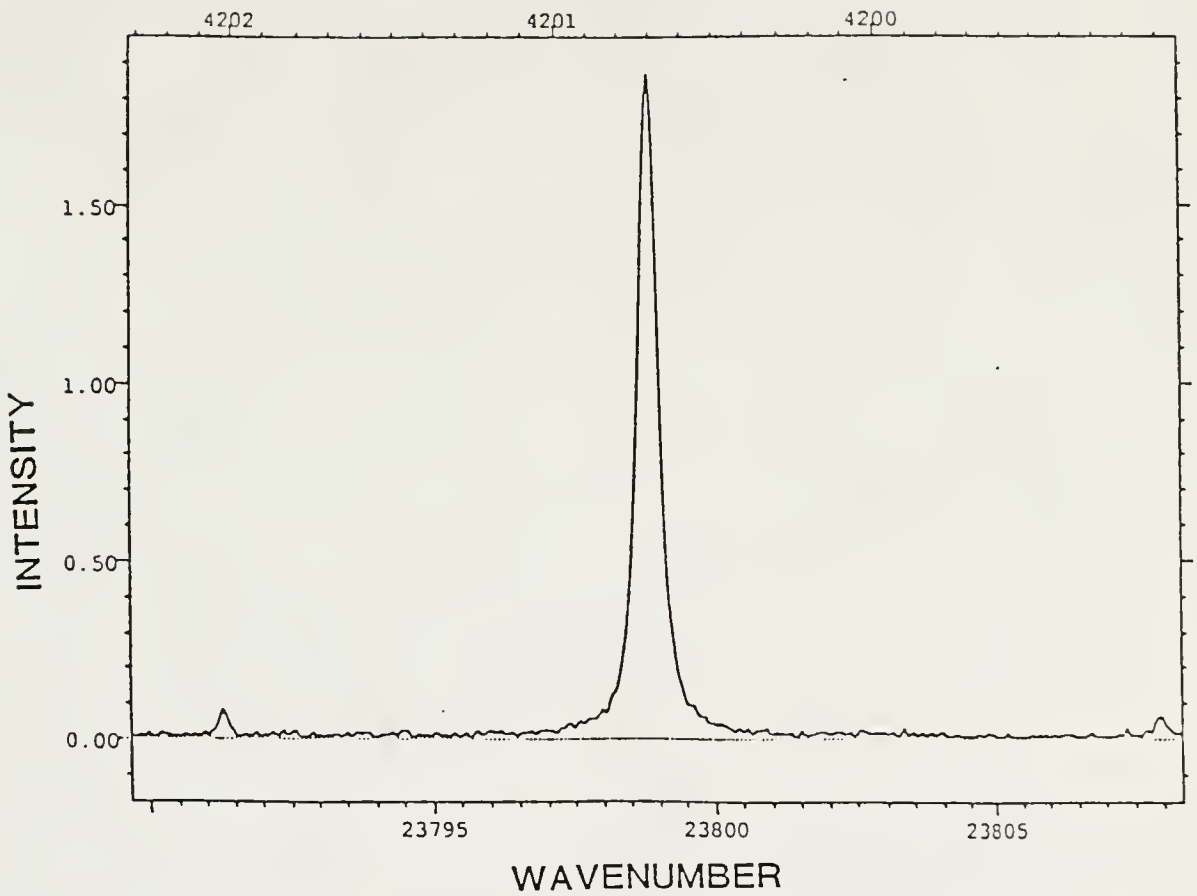
4202
4201
4200
1.50
1.00
0.50
0.00
INTENSITY
23795
23800
23805
WAVENUMBER

Figure 10. Line profile of Fe emission (1000 ppm) from analytical zone in ICP. (Top axis is in Å and the bottom is cm^{-1})

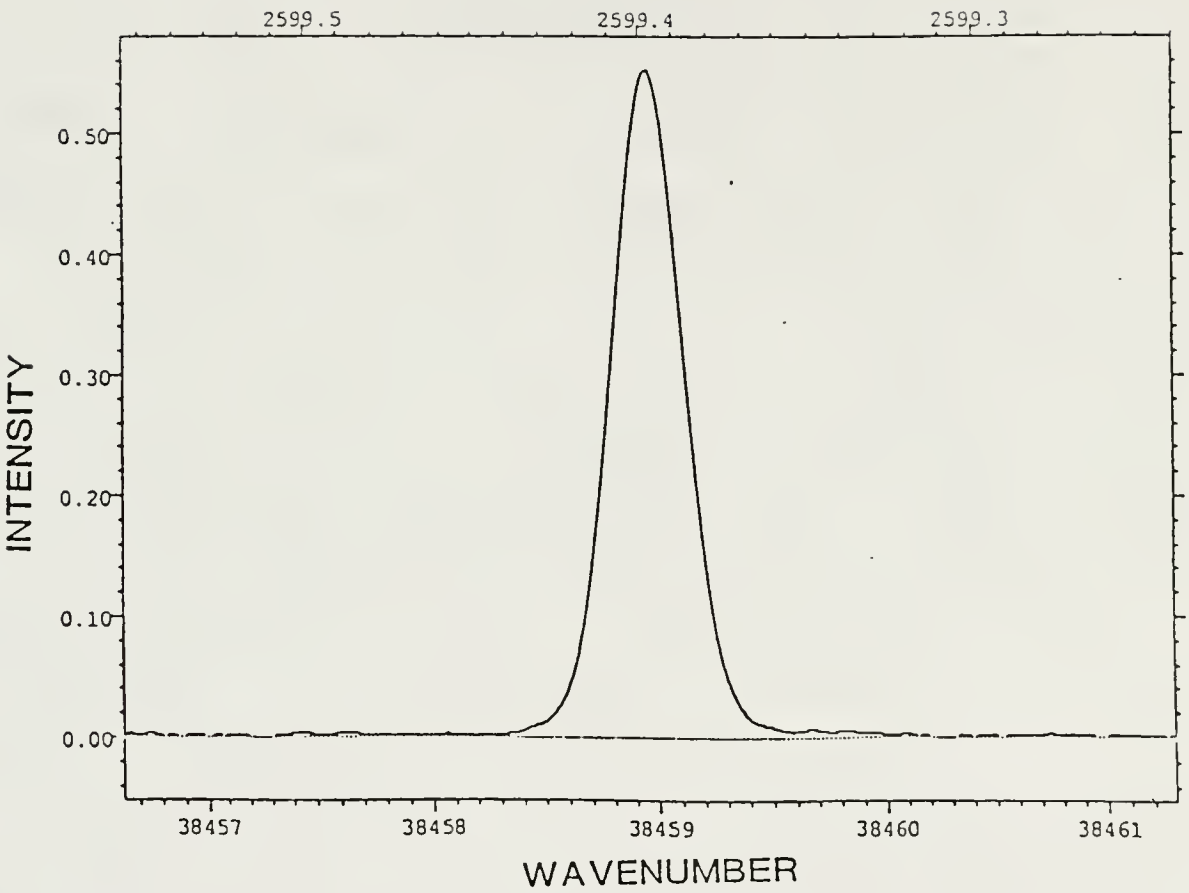
2599.5
2599.4
2599.3
0.50
0.40
0.30
0.20
0.10
0.00
INTENSITY
38457
38458
38459
38460
38461
WAVENUMBER

Figure 11. Diagram outlining the optical configuration of light sources (ICP and HCL) and optical components outside LAFTS.

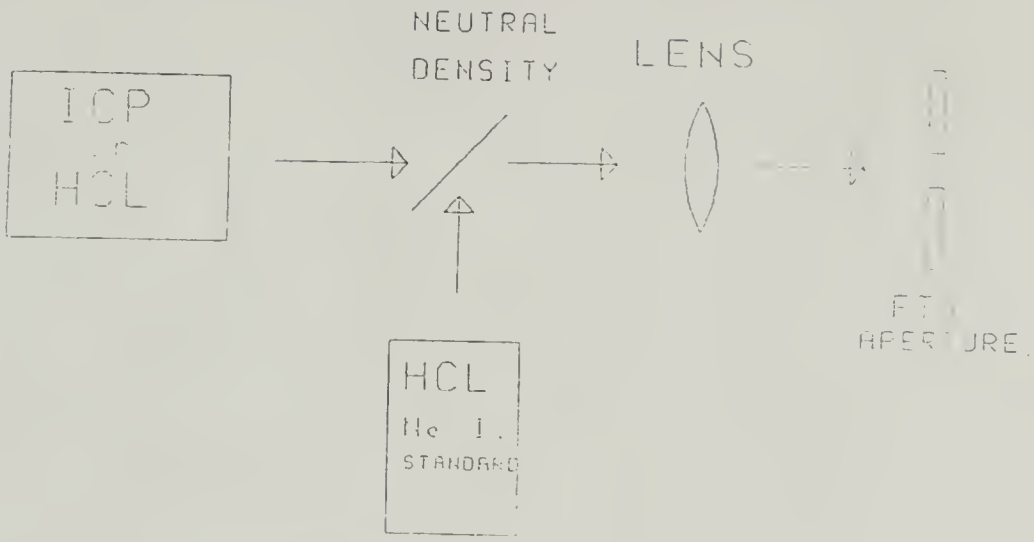
NEUTRAL
DENSITY
LENS
ICP
HCL
HCL
No 1.
STANDARD

Figure 12. The relationship between <r>, the average atomic radius, and the shift in the line position is demonstrated for 1.1 kW (*), 1.5 kW (+), and 1.9 kW (Δ). The <r> value is for the upper level and should be multiplied by the constant a_o (Bohr radius) for the correct approximation.

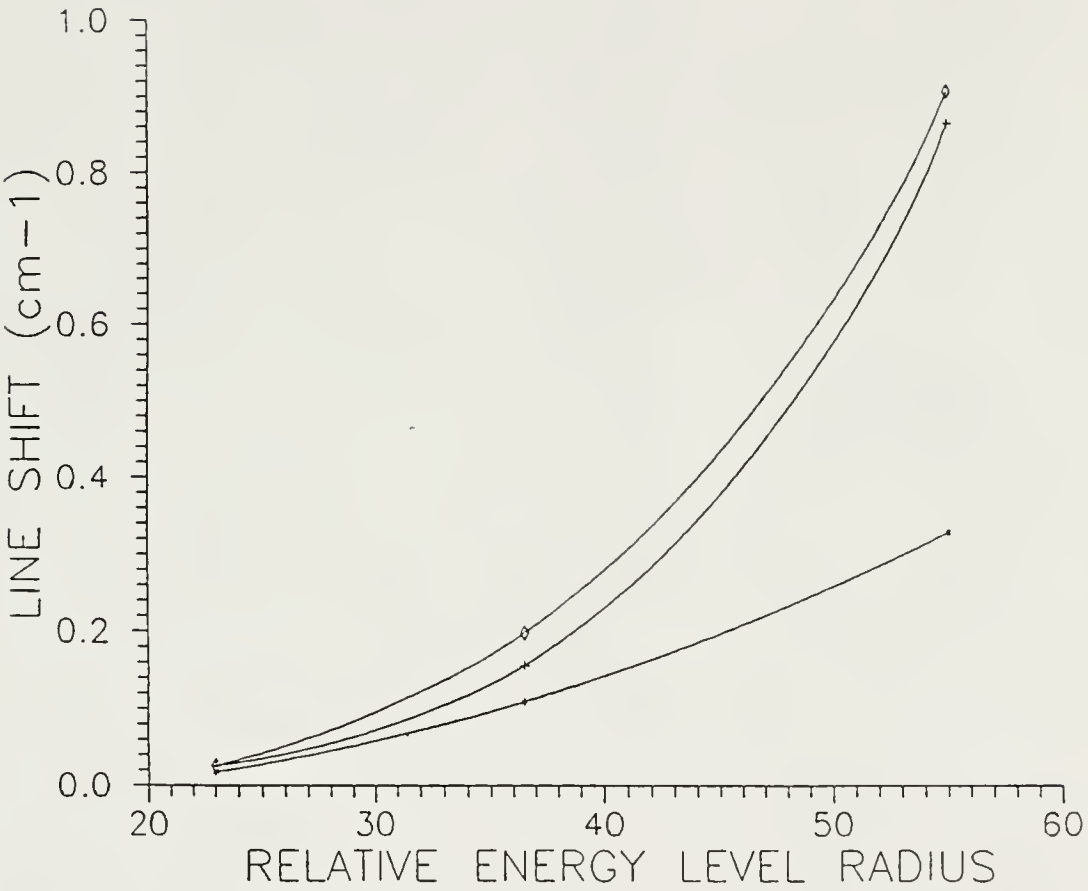
1.0
0.8
0.6
0.4
0.2
0.0
LINE SHIFT (cm-1)
20
30
40
50
60
RELATIVE ENERGY LEVEL RADIUS

Table 4. The transition, wavelength of transition, λ, line shift, $\Delta\lambda_s$, full width at half maximum (FWHM), $\Delta\lambda_T$, Doppler halfwidth, $\Delta\lambda_D$, Lorentzian halfwidth, $\Delta\lambda_L$, and the a- parameter of Ar emission from a 1.1 kW ICP. The Doppler temperature is 6500K. Positive shift values are red-shifted. Below each general transition (6p-4s, 5p-4s, 4p-4s) the average shift and standard deviation is tabulated.

Transition	λ (Å)	$\Delta\lambda_S$ (cm^{-1})	$\Delta\lambda_T$ (cm^{-1})	$\Delta\lambda_D$ (cm^{-1})	$\Delta\lambda_L$ (cm^{-1})	a
$6p[1.5]_2$-$4s[1.5]_2$	3555.	0.3446	0.6335	0.255	0.53	1.73
$6p[0.5]_0$-$4s[1.5]_1$	3607.	0.3136	0.6385	0.251	0.54	1.7
AVERAGE SHIFT (6p-4s)		0.3291 (±0.0219)				
$5p[0.5]_1$-$4s[1.5]_2$	3950.	0.1242	0.4405	0.229	0.32	1.16
$5p'[1.5]_2$-$4s[1.5]_1$	4045.	0.1038	0.3972	0.233	0.26	0.93
$5p[1.5]_2$-$4s[1.5]_2$	4159.	0.1154	0.4270	0.218	0.31	1.18
$5p[1.5]_1$-$4s[1.5]_2$	4165.	0.1104	0.4385	0.218	0.33	1.26
$5p'[0.5]_1$-$4s'[0.5]_0$	4183.	0.1383	0.4451	0.217	0.34	1.30
$5p[2.5]_2$-$4s[1.5]_2$	4191.	0.0957	0.3788	0.216	0.25	0.96
$5p'[1.5]_1$-$4s'[0.5]_0$	4192.	0.0984	0.3849	0.216	0.26	0.99
$5p[0.5]_0$-$4s[1.5]_1$	4199.	0.1243	0.4011	0.216	0.28	1.08
$5p[2.5]_3$-$4s[1.5]_2$	4201.	0.1063	0.5264	0.216	0.44	1.69
$5p[0.5]_1$-$4s[1.5]_2$	4252.	0.0807	0.3280	0.213	0.19	0.74
$5p[1.5]_2$-$4s[1.5]_1$	4267.	0.1417	0.3746	0.212	0.25	0.97
$5p[1.5]_1$-$4s[1.5]_1$	4273.	0.1046	0.3578	0.212	0.23	0.90
$5p[2.5]_2$-$4s[1.5]_1$	4301.	0.0976	0.3545	0.211	0.23	0.91
$5p'[1.5]_2$-$4s'[0.5]_1$	4334.	0.0972	0.4147	0.209	0.31	1.23

Table 4--continued.

$5p'[0.5]_1$-$4s'[0.5]_1$	4336.	0.0773	0.5441	0.209	0.46	1.83
$5p'[1.5]_1$-$4s'[0.5]_1$	4346.	0.1284	0.4080	0.209	0.30	1.19
$5p[0.5]_0$-$4s'[0.5]_1$	4511.	0.1179	0.3613	0.201	0.25	1.03
AVERAGE SHIFT (5p-4s)		0.1095 (±0.0182)				
$4p'[0.5]_1$-$4s[1.5]_2$	6967.	0.0179	0.1698	0.130	0.07	0.44
$4p'[1.5]_2$-$4s[1.5]_2$	7069.	0.0176	0.1610	0.128	0.06	0.39
AVERAGE SHIFT (4p-4s)		0.0177 (±0.0002)				

Table 5. The transition type, wavelength of transition, λ, line shift, $\Delta\lambda_s$, full width at half maximum (FWHM), $\Delta\lambda_T$, Doppler halfwidth, $\Delta\lambda_D$, Lorentzian halfwidth, $\Delta\lambda_L$, and the a-parameter of Ar emission from 1.5 kW ICP. The Doppler temperature is 6800 K. Positive shift values are red-shifted. Below each general transition (6p-4s, 5p-4s, 4p-4s) the average shift and standard deviation are tabulated.

Transition	λ (Å)	$\Delta\lambda_s$ (cm^{-1})	$\Delta\lambda_T$ (cm^{-1})	$\Delta\lambda_D$ (cm^{-1})	$\Delta\lambda_L$ (cm^{-1})	a
$6p[1.5]_2$-$4s[1.5]_2$	3555	0.5442	0.7807	0.261	0.69	2.20
$6p[0.5]_0$-$4s[1.5]_1$	3607	1.178	0.3333	0.257	0.13	0.42
AVERAGE SHIFT (6p-4s)		0.8610	(±0.4481)			
$5p[0.5]_1$-$4s[1.5]_2$	3950	0.1622	0.5703	0.235	0.47	1.66
$5p'[1.5]_2$-$4s[1.5]_1$	4045	0.1383	0.6131	0.229	0.53	1.92
$5p[1.5]_2$-$4s[1.5]_2$	4159	0.1703	0.4494	0.223	0.34	1.27
$5p[1.5]_1$-$4s[1.5]_2$	4165	0.1357	0.6745	0.222	0.60	2.24
$5p'[0.5]_1$-$4s'[0.5]_0$	4183	0.1715	0.5064	0.222	0.41	1.54
$5p[2.5]_2$-$4s[1.5]_2$	4191	0.1700	0.4185	0.221	0.30	1.13
$5p'[1.5]_1$-$4s'[0.5]_0$	4192	0.1578	0.4338	0.221	0.32	1.20
$5p[0.5]_0$-$4s[1.5]_1$	4199	0.1970	0.5339	0.221	0.44	1.66
$5p[2.5]_3$-$4s[1.5]_2$	4201	0.1528	0.4406	0.221	0.33	1.24
$5p[0.5]_1$-$4s[1.5]_2$	4252	0.0811	0.4219	0.218	0.31	1.18
$5p[1.5]_2$-$4s[1.5]_1$	4267	0.1708	0.4779	0.217	0.38	1.45
$5p[1.5]_1$-$4s[1.5]_1$	4273	0.1606	0.4202	0.217	0.31	1.19
$5p[2.5]_2$-$4s[1.5]_1$	4301	0.1562	0.5351	0.216	0.45	1.74
$5p'[1.5]_2$-$4s'[0.5]_1$	4334	0.1219	0.8084	0.214	0.75	2.41

Table 5--continued.

$5p'[0.5]_1$-$4s'[0.5]_1$	4336	0.1350	0.5421	0.213	0.44	1.77
$5p'[1.5]_1$-$4s'[0.5]_1$	4346	0.1797	0.5264	0.213	0.44	1.71
$5p[0.5]_0$-$4s'[0.5]_1$	4511	0.1979	0.4068	0.206	0.30	1.21
AVERAGE SHIFT (5p-4s)		0.1564 (±0.0283)				
$4p'[0.5]_1$-$4s[1.5]_2$	6967	0.0204	0.1801	0.133	0.08	0.499
$4p'[1.5]_2$-$4s[1.5]_2$	7069	0.0305	0.1801	0.131	0.09	0.571
AVERAGE SHIFT (4p-4s)		0.0254 (±0.0071)				

Table 6.The transition type, wavelength of transition, λ,line shift, $\Delta\lambda_s$, full width at half maximum (FWHM), $\Delta\lambda_T$, Doppler contribution, $\Delta\lambda_D$, Lorentzian contribution, $\Delta\lambda_L$, and the a-parameter of Ar emission from a 1.9 kW ICP. The Doppler temperature is 7100 K. Positive shift values are redshifted. Below each general transition (6p-4s, 5p-4s, 4p-4s) the average shift and standard deviation are tabulated.

Transition	λ (Å)	$\Delta\lambda_S$ (cm^{-1})	$\Delta\lambda_T$ (cm^{-1})	$\Delta\lambda_D$ (cm^{-1})	$\Delta\lambda_L$	a
$6p[1.5]_2$-$4s[1.5]_2$	3555	0.6432	0.5962	0.266	0.48	1.49
$6p[0.5]_0$-$4s[1.5]_1$	3607	1.165	0.3068	0.263	0.08	0.25
AVERAGE SHIFT (6p-4s)		0.9040	(±3680)			
$5p[0.5]_1$-$4s[1.5]_2$	3950	0.2409	0.5762	0.239	0.48	1.66
$5p'[1.5]_2$-$4s[1.5]_1$	4045	0.1869	0.5261	0.234	0.42	1.49
$5p[1.5]_2$-$4s[1.5]_2$	4159	0.2064	0.5011	0.227	0.40	1.46
$5p[1.5]_1$-$4s[1.5]_2$	4165	0.1894	0.4608	0.227	0.35	1.28
$5p'[0.5]_1$-$4s'[0.5]_0$	4183	0.2152	0.7554	0.226	0.69	2.53
$5p[2.5]_2$-$4s[1.5]_2$	4191	0.1635	0.4865	0.226	0.38	1.40
$5p'[1.5]_1$-$4s'[0.5]_0$	4192	0.1587	0.4689	0.226	0.36	1.32
$5p[0.5]_0$-$4s[1.5]_1$	4199	0.2129	0.8689	0.226	0.81	2.98
$5p[2.5]_3$-$4s[1.5]_2$	4201	0.1765	1.2200	0.225	1.18	4.35
$5p[0.5]_1$-$4s[1.5]_2$	4252	0.1812	0.4081	0.223	0.29	1.08
$5p[1.5]_2$-$4s[1.5]_1$	4267	0.2300	0.5035	0.222	0.40	1.50
$5p[1.5]_1$-$4s[1.5]_1$	4273	0.1630	0.5839	0.222	0.50	1.87
$5p[2.5]_2$-$4s[1.5]_1$	4301	0.1952	0.4673	0.220	0.36	1.36

Table 6--continued.

$5p'[1.5]_2$-$4s'[0.5]_1$	4334	0.1699	0.5565	0.218	0.47	1.79
$5p'[0.5]_1$-$4s'[0.5]_1$	4336	0.2405	0.7283	0.218	0.66	2.51
$5p'[1.5]_1$-$4s'[0.5]_1$	4346	0.1662	0.4559	0.218	0.35	1.33
$5p[0.5]_0$-$4s'[0.5]_1$	4511	0.2759	0.6060	0.210	0.53	2.09
AVERAGE SHIFT (5p-4s)		0.1983 (±0.0335)				
$4p'[0.5]_1$-$4s[1.5]_2$	6967	0.0261	0.1967	0.136	0.10	0.612
$4p'[1.5]_2$-$4s[1.5]_2$	7069	0.0261	0.2098	0.134	0.13	0.807
AVERAGE SHIFT (4p-4s)		0.0261 (±0.000)				

Table 7. The transition type, wavelength of transition, λ, line shift, $\Delta\lambda_S$, full width at half maximum (FWHM), $\Delta\lambda_T$, Doppler contribution, $\Delta\lambda_D$, Lorentzian contribution, $\Delta\lambda_L$, and the a-parameter of Fe emission from a 1.1 kW ICP. The Doppler temperature is 6000 K and the electron density 1.20×10^{15} cm^{-3}. Positive shift values are red-shifted. For this table, the average line shift is 0.0185 cm^{-1} with a standard deviation of 0.0062 cm^{-1}. The concentration of iron aspirated into the ICP was 1000 μg/ml.

Transition		λ (Å)	$\Delta\lambda_S$ (cm^{-1})	$\Delta\lambda_T$ (cm^{-1})	$\Delta\lambda_D$ (cm^{-1})	$\Delta\lambda_L$ (cm^{-1})	a
$a^4D - z^4F^\circ$	II	2755.73	0.0452	0.3394	0.274	0.12	0.364
$a^5D - y^5F^\circ$	I	2966.90	0.0181	0.3200	0.254	0.12	0.392
$a^5D - y^5D^\circ$	I	2994.43	0.0220	0.3144	0.252	0.11	0.363
$a^5D - y^5D^\circ$	I	3021.07	0.0232	0.3091	0.249	0.11	0.366
$a^5D - y^5D^\circ$	I	3047.60	0.0201	0.3265	0.248	0.14	0.470
$a^5D - y^5D^\circ$	I	3059.09	0.0172	0.3474	0.247	0.17	0.573
$a^5D - z^5P^\circ$	I	3440.99	0.0154	0.2646	0.219	0.08	0.303
$a^5F - z^3G^\circ$	I	3565.38	0.0190	0.2605	0.212	0.09	0.353
$a^5F - z^5G^\circ$	I	3581.19	0.0194	0.2601	0.211	0.09	0.355
$a^5F - z^5G^\circ$	I	3608.86	0.0168	0.2599	0.209	0.09	0.357
$a^5F - z^5G^\circ$	I	3618.77	0.0199	0.2849	0.208	0.13	0.518
$a^5F - z^5G^\circ$	I	3631.46	0.0175	0.2555	0.208	0.09	0.360
$a^5F - z^5G^\circ$	I	3647.84	0.0183	0.2784	0.207	0.12	0.482
$a^5D - z^5F^\circ$	I	3719.93	0.0127	0.2447	0.203	0.08	0.328
$a^5D - z^5F^\circ$	I	3745.56	0.0112	0.2470	0.201	0.08	0.330
$a^5D - z^5F^\circ$	I	3748.26	0.0119	0.2472	0.201	0.08	0.330
$a^5F - y^5F^\circ$	I	3758.23	0.0187	0.2466	0.201	0.08	0.331

Table 7--continued.

$a^5F - y^5F^\circ$	I	3763.79	0.0179	0.2460	0.200	0.08	0.332
$a^3F - y^3D^\circ$	I	3815.84	0.0221	0.2477	0.197	0.09	0.378
$a^5F - y^5D^\circ$	I	3820.43	0.0184	0.2574	0.197	0.11	0.463
$a^5F - y^5D^\circ$	I	3825.88	0.0194	0.2439	0.197	0.09	0.374
$a^5F - y^5D^\circ$	I	3834.22	0.0165	0.2437	0.197	0.09	0.380
$a^5D - z^5D^\circ$	I	3859.91	0.0122	0.2368	0.196	0.08	0.340
$a^5D - z^5D^\circ$	I	3886.28	0.0113	0.2324	0.194	0.07	0.299
$a^3F - y^3F^\circ$	I	4045.82	0.0192	0.3011	0.186	0.19	0.847
$a^3F - y^3F^\circ$	I	4063.60	0.0222	0.2263	0.186	0.08	0.358
$a^3F - z^5G^\circ$	I	4383.55	0.0148	0.2173	0.172	0.08	0.386
$a^3F - z^5G^\circ$	I	4404.75	0.0165	0.2151	0.171	0.08	0.388

Table 8. The transition type, wavelength of transition, λ, line shift, $\Delta\lambda_S$, full width at half maximum (FWHM), $\Delta\lambda_T$, Doppler, $\Delta\lambda_D$, Lorentzian , $\Delta\lambda_L$, and the a-parameter of Fe emission from a 1.5 kW ICP. The Doppler temperature is 6200 K and the electron density is 2.05×10^{15} cm^{-3}. Positive shift values are red-shifted. The average shift value for this table is 0.0188 cm^{-1} with a standard deviation of 0.0066 cm^{-1}. 1000 μg/ml Fe solution was aspirated into the ICP.

Transition		λ (Å)	$\Delta\lambda_s$ (cm^{-1})	$\Delta\lambda_T$ (cm^{-1})	$\Delta\lambda_D$ (cm^{-1})	$\Delta\lambda_L$ (cm^{-1})	a
$a^4D - z^4F^o$	II	2755.73	0.0431	0.3615	0.273	0.15	0.455
$a^5D - y^5F^o$	I	2966.90	0.0173	0.3290	0.254	0.13	0.425
$a^5D - y^5D^o$	I	2994.43	0.0255	0.3349	0.252	0.14	0.462
$a^5D - y^5D^o$	I	3021.07	0.0148	0.3115	0.250	0.11	0.366
$a^5D - y^5D^o$	I	3047.60	0.0277	0.3251	0.247	0.14	0.470
$a^5D - y^5D^o$	I	3059.09	0.0124	0.3262	0.247	0.14	0.472
$a^5D - z^5P^o$	I	3440.99	0.0214	0.2827	0.219	0.11	0.417
$a^5F - z^3G^o$	I	3565.38	0.0218	0.2766	0.212	0.10	0.384
$a^5F - z^5G^o$	I	3581.19	0.0209	0.2731	0.211	0.11	0.434
$a^5F - z^5G^o$	I	3608.86	0.0199	0.2716	0.209	0.11	0.437
$a^5F - z^5G^o$	I	3618.77	0.0198	0.2689	0.209	0.11	0.439
$a^5F - z^5G^o$	I	3631.46	0.0188	0.2786	0.208	0.12	0.480
$a^5F - z^5G^o$	I	3647.84	0.0160	0.2639	0.207	0.10	0.402
$a^5D - z^5F^o$	I	3719.93	0.0134	0.2963	0.203	0.16	0.656
$a^5D - z^5F^o$	I	3745.56	0.0146	0.2497	0.202	0.09	0.371
$a^5D - z^5F^o$	I	3748.26	0.0097	0.2575	0.201	0.10	0.431
$a^5F - y^5F^o$	I	3758.23	0.0232	0.3186	0.201	0.19	0.787

Table 8--continued.

$a^5F - y^5F^\circ$	I	3763.79	0.0132	0.2509	0.201	0.09	0.373
$a^3F - y^3D^\circ$	I	3815.84	0.0205	0.2625	0.198	0.11	0.462
$a^5F - y^5D^\circ$	I	3820.43	0.0181	0.2820	0.197	0.14	0.589
$a^5F - y^5D^\circ$	I	3825.88	0.0191	0.2542	0.197	0.10	0.422
$a^5F - y^5D^\circ$	I	3834.22	0.0196	0.2476	0.197	0.09	0.380
$a^5D - z^5D^\circ$	I	3859.91	0.0108	0.2429	0.195	0.09	0.382
$a^5D - z^5D^\circ$	I	3886.28	0.0231	0.2651	0.194	0.12	0.514
$a^3F - y^3F^\circ$	I	4045.82	0.0137	0.2445	0.186	0.10	0.446
$a^3F - y^3F^\circ$	I	4063.60	0.0115	0.2707	0.186	0.14	0.627
$a^3F - z^5G^\circ$	I	4383.55	0.0146	0.2208	0.172	0.09	0.434
$a^3F - z^5G^\circ$	I	4404.75	0.0211	0.2529	0.171	0.14	0.679

Table 9. The transition type, wavelength of transition, λ, line shift, $\Delta\lambda_S$, full width at half maximum (FWHM), $\Delta\lambda_T$, Doppler contribution, $\Delta\lambda_D$, Lorentzian contribution, $\Delta\lambda_L$, and the a-parameter of Fe emission from a 1.9 kW ICP. The Doppler temperature is 6500 K and the electron density is 2.85×10^{15} cm^{-3}. Positive shift values are red-shifted. The average shift for all lines listed in this table is 0.0176 cm^{-1} with a standard deviation of 0.0132 cm^{-1}. The concentration of Fe aspirated into the ICP was 1000 μg/ml.

Transition		λ (Å)	$\Delta\lambda_S$ (cm^{-1})	$\Delta\lambda_T$ (cm^{-1})	$\Delta\lambda_D$ (cm^{-1})	$\Delta\lambda_L$ (cm^{-1})	a
$a^4D - z^4F^o$	II	2755.73	0.0390	0.5696	0.284	0.42	1.23
$a^5D - y^5F^o$	I	2966.90	0.0249	0.3240	0.264	0.11	0.36
$a^5D - y^5D^o$	I	2994.43	0.0544	0.4185	0.262	0.25	0.79
$a^5D - y^5D^o$	I	3021.07	0.0116	0.3210	0.259	0.11	0.35
$a^5D - y^5D^o$	I	3047.60	0.0226	0.3560	0.257	0.17	0.55
$a^5D - y^5D^o$	I	3059.09	0.0157	0.3155	0.256	0.11	0.35
$a^5D - z^5P^o$	I	3440.99	-0.0109	0.3246	0.228	0.16	0.58
$a^5F - z^3G^o$	I	3565.38	0.0305	0.2661	0.220	0.09	0.34
$a^5F - z^5G^o$	I	3581.19	0.0221	0.2872	0.219	0.12	0.45
$a^5F - z^5G^o$	I	3608.86	0.0188	0.2592	0.217	0.08	0.31
$a^5F - z^5G^o$	I	3618.77	0.0105	0.2641	0.217	0.09	0.34
$a^5F - z^5G^o$	I	3631.46	0.0386	0.2796	0.216	0.11	0.42
$a^5F - z^5G^o$	I	3647.84	0.0101	0.2652	0.215	0.09	0.35
$a^5D - z^5F^o$	I	3719.93	0.0164	0.2617	0.211	0.09	0.35
$a^5D - z^5F^o$	I	3745.56	0.0210	0.3310	0.209	0.20	0.79
$a^5D - z^5F^o$	I	3748.26	0.0140	0.2507	0.209	0.08	0.32
$a^5F - y^5F^o$	I	3758.23	0.0188	0.3103	0.207	0.17	0.68
$a^5F - y^5F^o$	I	3763.79	0.0193	0.2912	0.208	0.14	0.56

Table 9--continued.

$a^3F - y^3D^\circ$	I	3815.84	0.0135	0.3395	0.205	0.21	0.85
$a^5F - y^5D^\circ$	I	3820.43	0.0176	0.2575	0.205	0.09	0.36
$a^5F - y^5D^\circ$	I	3825.88	0.0152	0.2599	0.205	0.10	0.41
$a^5F - y^5D^\circ$	I	3834.22	0.0266	0.4480	0.204	0.35	1.42
$a^5D - z^5D^\circ$	I	3859.91	0.0089	0.2895	0.203	0.15	0.61
$a^5D - z^5D^\circ$	I	3886.28	0.0081	0.2760	0.202	0.13	0.53
$a^3F - y^3F^\circ$	I	4045.82	0.0118	0.2508	0.194	0.10	0.43
$a^3F - y^3F^\circ$	I	4063.60	0.0076	0.2509	0.193	0.10	0.43
$a^3F - z^5G^\circ$	I	4383.55	0.0165	0.2426	0.178	0.11	0.51
$a^3F - z^5G^\circ$	I	4404.75	-0.0102	0.2338	0.178	0.10	0.47

Table 10. The transition type, wavelength of transition, λ, line shift, $\Delta\lambda_S$, full width at half maximum (FWHM), $\Delta\lambda_T$, Doppler contribution, $\Delta\lambda_D$, Lorentzian contribution, $\Delta\lambda_L$, and the a-parameter of Ar emission from a 1.1 kW ICP. The Doppler temperature is 6500 K. Positive shift values are red-shifted.

Transition	λ (Å)	$\Delta\lambda_S$ (cm^{-1})	$\Delta\lambda_T$ (cm^{-1})	$\Delta\lambda_D$ (cm^{-1})	$\Delta\lambda_L$ (cm^{-1})	a
$4p[0.5]_1$-$4s'[0.5]_0$	10472.	0.0159	0.1365	0.0865	0.08	0.77
$4p[2.5]_2$-$4s'[0.5]_1$	9787.	0.0172	0.1934	0.0926	0.15	1.35
$4p[0.5]_1$-$4s[1.5]_1$	9660.	0.0121	0.1389	0.0938	0.08	0.71
$4p[1.5]_1$-$4s'[0.5]_1$	9356	0.0050	0.1963	0.0969	0.15	1.29
$4p[1.5]_2$-$4s'[0.5]_1$	9227.	0.0189	0.1999	0.0983	0.15	1.27
$4p[0.5]_1$-$4s\ [1.5]_2$	9125.	0.0042	0.1419	0.0994	0.07	0.59
$4p[1.5]_1$-$4s'[0.5]_0$	8670.	0.0268	0.1506	0.1046	0.08	0.64
$4p'[1.5]_1$-$4s'[0.5]_1$	8523.	0.0151	0.2092	0.1064	0.16	1.25
$4p[2.5]_2$-$4s[1.5]_1$	8427.	0.0016	0.1677	0.1076	0.10	0.77
$4p'[1.5]_2$-$4s'[0.5]_1$	8410.	0.0164	0.2250	0.1078	0.18	1.39
$4p'[0.5]_1$-$4s'[0.5]_1$	8266.	0.0183	0.2125	0.1097	0.16	1.21
$4p[2.5]_3$-$4s[1.5]_2$	8117.	-0.011	0.1833	0.1117	0.12	0.89
$4p[1.5]_1$-$4s[1.5]_1$	8105.	0.0217	0.1686	0.1118	0.10	0.74
$4p[2.5]_2$-$4s[1.5]_2$	8016.	0.0216	0.1602	0.1131	0.08	0.59
$4p[1.5]_2$-$4s[1.5]_1$	8008.	0.0248	0.1652	0.1132	0.09	0.66
$4p'[1.5]_1$-$4s'[0.5]_0$	7950.	0.0254	0.1610	0.1140	0.08	0.58
$4p'[0.5]_1$-$4s'[0.5]_0$	7726.	0.0269	0.1658	0.1173	0.08	0.57
$4p[1.5]_1$-$4s[1.5]_2$	7725.	0.0230	0.1710	0.1174	0.09	0.64
$4p[1.5]_2$-$4s[1.5]_2$	7637.	0.0463	0.1683	0.1187	0.09	0.63
$4p[0.5]_0$-$4s[1.5]_1$	7515.	0.0280	0.1851	0.1206	0.11	0.79

Table 10--continued.

$4p'[0.5]_0$-$4s'[0.5]_1$	7505.	0.0301	0.2297	0.1208	0.17	1.17
$4p'[1.5]_2$-$4s[1.5]_1$	7386.	0.0224	0.1785	0.1227	0.10	0.65
$4p'[0.5]_1$-$4s[1.5]_1$	7274.	0.0255	0.1806	0.1246	0.10	0.68
$4p'[1.5]_2$-$4s[1.5]_2$	7069.	0.0241	0.1756	0.1301	0.09	0.57
$4p'[0.5]_1$-$4s[1.5]_2$	6967.	0.0260	0.1783	0.1301	0.09	0.57

Table 11. Line shifts, $\Delta\nu$, of Ca, Sr, and Ba in 1.1 Kw ICP. The wavenumber positions, ν, for hollow cathode lamp (standard, nonshifted) verses the ICP emission. The Doppler temperature is 6000 K and the electron density is 1.20×10^{15} cm^{-3} for the ICP. Wavenumber positions given are calibrated against a Ne I standard for absolute values. Negative values are blue-shifted.

ELEMENT	ν (HCL) (cm^{-1})	ν (ICP) (cm^{-1})	$\Delta\nu_s$ (cm^{-1})
Barium II	20261.5370	20261.5479	-0.0109
Barium II	21952.3718	21952.3975	-0.0257
Calcium II	25191.5197	25191.5241	-0.0044
Calcium II	25414.4307	25414.4147	0.0160
Strontium II	24516.5792	24516.5870	-0.0078

CHAPTER 6
A VARIABLE BANDPASS FILTER FOR ULTRAVIOLET/VISIBLE FOURIER TRANSFORM SPECTROSCOPY

Introduction

Fourier Transform Spectroscopy (FTS) has several advantages over grating and prism spectrometers. Included in these are wavenumber precision and accuracy, intensity precision, and resolving power. Detrimental to the FT technique is the multiplex disadvantage (7,82), which arises from shot and/or flicker noises at detected wavelengths other than the analytical wavelength hitting the detector causing a decreased signal-to-noise ratio compared to a single slit scanning dispersive spectrometer system. This disadvantage is more prominent in FT-UV/VIS then in FT-IR studies. In FT studies involving a continuum source, this disadvantage can become severe. The Inductively Coupled Plasma (ICP), Direct Current Plasma (DCP), and absorbance techniques utilizing a white light are examples of light sources that can magnify the multiplex disadvantage.

In our research (83), the Los Alamos Fourier Transform Spectrometer is used to measure Stark shifts in wavenumber positions of atoms and ions from a 27.12 MHz atmospheric pressure argon Inductively Coupled Plasma (ICP). The line

positions of atoms and ions in the ICP are compared to the unshifted line positions of the same species in a commercial hollow cathode lamp (HCL). To achieve adequate wavenumber positions (1 part in $4x10^8$), the lines analyzed need good signal-to-noise ratios (SNRs). Both the HCL and ICP emit numerous spectral lines. The ICP, being a hotter source, has considerable ion line emission. The HCL, with Doppler temperatures typically 1/10 that of the ICP (6000 K vs 600 K) has considerable atom line emission, particularly the fill gas emission in the near infrared. In such measurements of Stark shifted line positions, we find that the data set available is small for two reasons. First, the difference in source emission intensities between the same lines emitted from the ICP and the HCL reduces the number of lines available for comparison. Second, the multiplex disadvantage will substantially reduce the SNR of all lines.

A single filter with two features is desired. First, the ability to vary the bandpass of the filter over a wide range. Second, the ability to select the wavenumber region observed over a wide range. Optical filters do not meet our specifications for two reasons; the bandpass allowed rarely matches the needs desired, and the transmission of these optical filters often increases in the near IR resulting in excessive shot noise from spectral lines/bands in this region. Our sources (HCL, ICP) use inert gases having strong emission in the near IR region, resulting in a serious deterioration

of the SNR for lines observed in the ultraviolet and visible.

Hirschfeld and Chase (84) and Hirschfeld and Milanovich (85) summarized several techniques that could be used to overcome problems associated with excess light in FT-Raman experiments. One of these is the use of a nonscanning subtractive dispersive double monochromator. This filtering approach has been shown to be a valuable tool for micro-Raman work (85). We have adapted this filter for use as a bandpass filter in FT-continuum source work. We demonstrate the feasibility of this filter using a white light source.

Experimental

Figure 13 shows the configuration of the experiment. A Bomem DA-3 is used at low resolution (30 cm^{-1}) for this study. The gratings (G1, G2) are manufactured by Instrumental SA. Both are blazed for 700 nm (1200 grooves/mm, 25 mm x 25 mm). F numbers of the input lens (L3) and FTS are matched. The white light source (W.L.), gratings, lens-1 (L1) and lens-3 (L3) are held constant for all experiments. The mirrors (M1,M2), lens-2 (L2) aperture-2 (A2) are varied for selective purposes. L1 serves to collimate the light source. A1 (5 mm diameter) and A3 (3-10 mm diameter) are circular apertures. For A1, we use an aperture as opposed to a slit to maintain some of the throughput advantage of the FTS for emission studies. Since we are looking at relatively large bandpasses (> 500 cm^{-1}), the loss in spectral resolution of an aperture

verses a slit is not significant. G1 and G2 are mounted back to back. A2 serves to block unwanted light and to let through a preset band. A2 is rectangular; A2 and L2 are moved laterally to select both wavenumber region and bandpass. M1 and M2 are matched concave mirrors, where M1 transfer the range of nearly collimated radiation selected by A2-L2 and M2 transfers that range of nearly collimated light on to the surface of G2 which further disperses and transfers the band of nearly collimated radiation into L3-A3 where A3 is the aperture to the FTS.

The bandpass can be adjusted by changing the diameter of A2 and/or the distance of A2 from G1. Narrower bandpasses can be achieved with smaller apertures (A1, A2) at greater distances (A2 from G1). Decreasing the apertures (A1, A2) decreased the photon flux entering the FTS and therefore decreases the multiplex disadvantage. Moving A2-L2 perpendicular to the nearly collimated light reaching M1 resulted in a change in the central wavelength of the band passed.

The distances between optical components varied slightly depending on central wavenumber and bandpass selection. Approximate dimensions are as follows: L1-A1, 1 cm; A1-Grating 1, 11 cm; Grating 1-A2, 12 cm; M1-M2, 26 cm; Grating 2-L3, 12 cm.

Results

Figure 14 shows two spectra (25 scans) of the filtered white light source with a 2000 cm^{-1} bandpass. The strong narrow line in both is the He-Ne (6328 A) laser leakage and is used as a visual reference for alignment of the optics A1-G1-A2-L2-M1-M2-G2-L3-A3. For this demonstration the central wavenumber shifts from approximately 15000 cm^{-1} to 16000 cm^{-1}.

Figure 15 shows a narrower bandpass (approximately 1000 cm^{-1}) that varied from 16500 to 18700 cm^{-1} in four windows. The gratings performance fell off above 20000 cm^{-1} and visual alignment of the optics in Figure 13 below 13000 cm^{-1} becomes difficult by eye; an infrared sensor is needed to see the radiation. This justified the range (13000-19000 cm^{-1}) demonstrated here.

Conclusion

A bandpass filter which varied both wavenumber position and bandpass and provide a limited spectral range is demonstrated. The bandpass filter is being developed the filter for FT-UV/VIS source studies. The filter removed unwanted light which affected the quality of broad band multiple line spectra. Removal of the prominent lines of neon or argon appearing in the 600-900 nm range in hollow cathode lamp (HCL) emission is also of interest to us. These lines are often the most intense in HCL emission studies. Optical filters have two disadvantages which often arise in studies of

this sort. First the bandpass of the optical filter may not match the desired need, especially in the ultraviolet. Second, transmission of these filters often increases in the NIR (above 900 nm) and allows the fill gas emission (particularly Ar) to enter the FTS. Our aim is to replace optical filters with a simple filter that allows variation in both position and bandpass of the filter.

We should note that a variety of derivations of this filter are possible. For example, replacing M1 and M2 with parabolic mirrors would allow the removal of L2. M1 and M2 would collimate and reflect the radiation to G2 eliminating the need for L2.

Figure 13. Outline of bandpass filter. (W.L. = white light, A = aperture, G = grating)

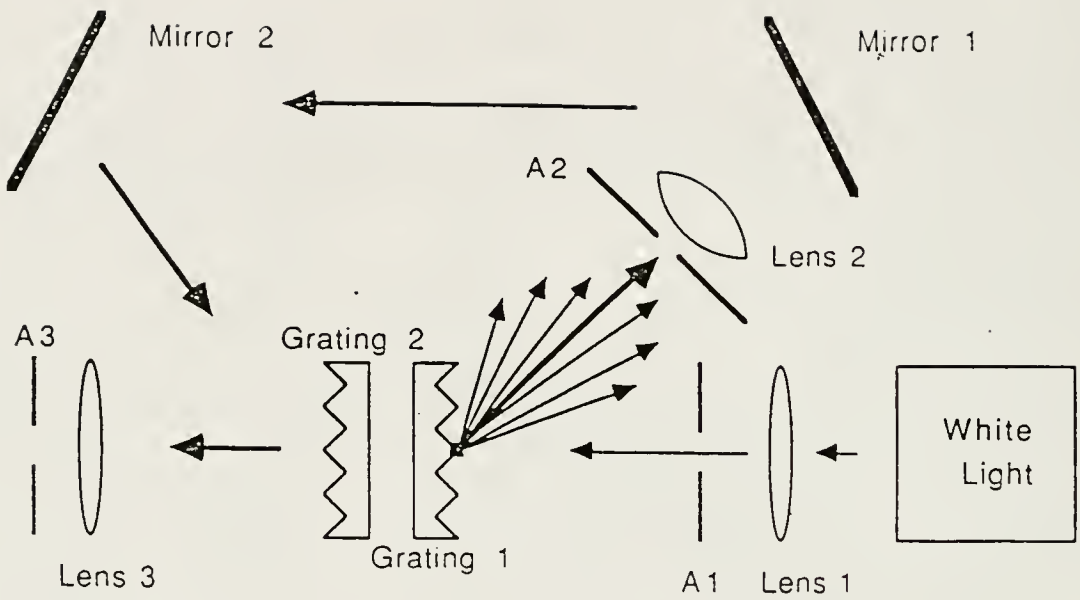
Mirror 2
Mirror 1
A2
Lens 2
A3
Grating 2
White
Light
Grating 1
Lens 3
A1
Lens 1

Figure 14. 2000 cm^{-1} bandpass of filtered white light source centered at 15000 cm^{-1} (top) and 16000 cm^{-1} (bottom). Sharp line (6328 A) is He-Ne laser leakage from Bomem FTS alignment system.

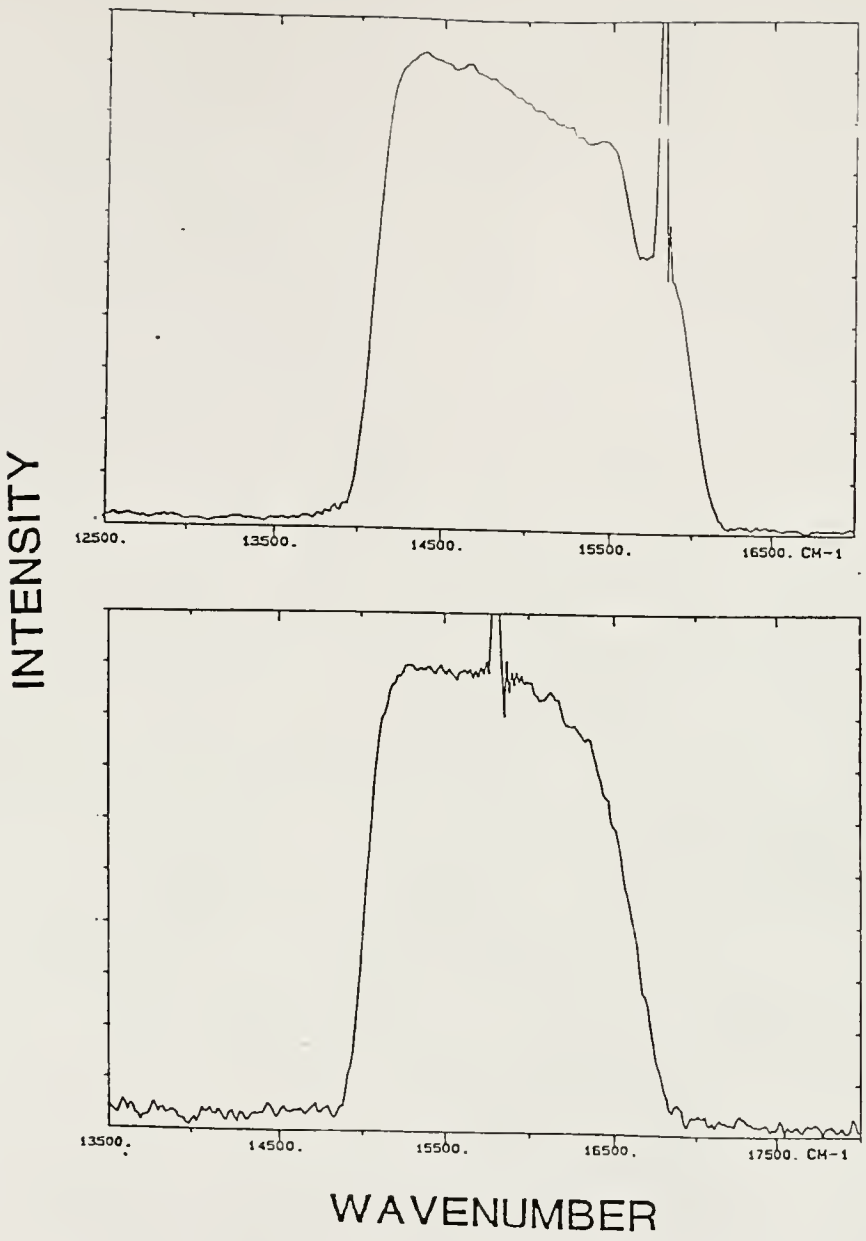
INTENSITY
12500.
13500.
14500.
15500.
16500. CM-1
13500.
14500.
15500.
16500.
17500. CM-1
WAVENUMBER

Figure 15. 1000 cm^{-1} bandpass centered at 16600 cm^{-1} (1), 17300 cm^{-1} (2), 17800 cm^{-1} (3), 18750 cm^{-1} (4).

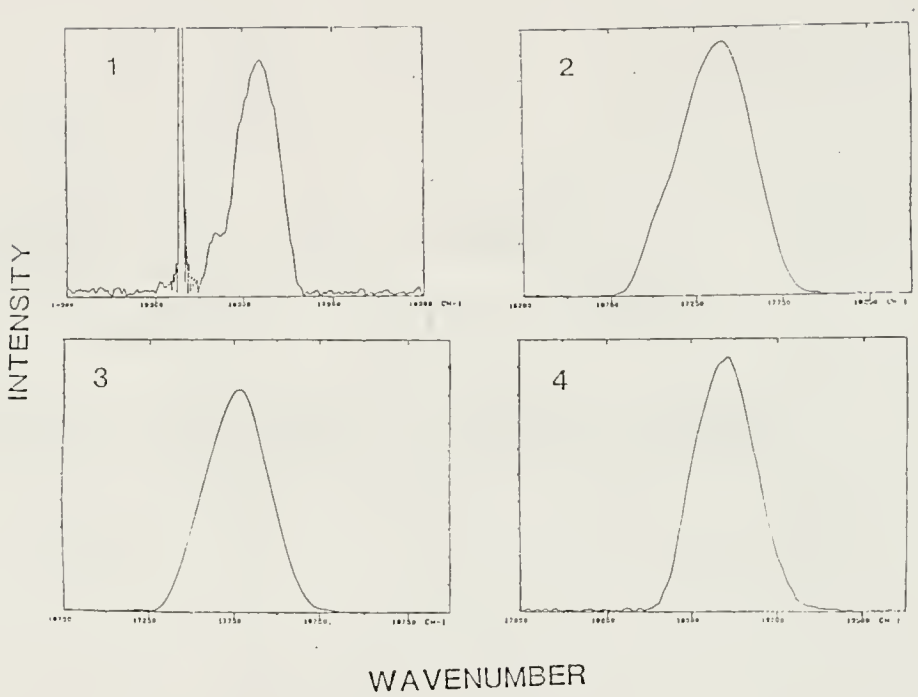
1
2
3
4
INTENSITY
WAVENUMBER

CHAPTER 7
A PROPOSED WAVENUMBER, INTENSITY, AND RESOLUTION STANDARD FOR HIGH RESOLUTION UV/VIS FOURIER TRANSFORM SPECTROSCOPY

Introduction

In this chapter, using Re I (527.55 nm) as a standard for measuring the quality of spectra obtained with a Fourier Transform Spectrometer (FTS) operating in the ultraviolet and visible is proposed. In addition to the multiplex and throughput advantages, three additional advantages for FT-UV/VIS are resolution, intensity precision and accuracy, and wavenumber precision and accuracy. The Re I (527.55 nm) line, which has hyperfine structure (HFS) and isotope shifts (IS), offers an excellent reference standard for measuring the above mentioned qualities. Quite often FT-UV/VIS instruments claim achieving resolutions ($\Delta\nu$, cm^{-1}) based simply on mirror displacement (L, cm) where

$$\Delta\nu = 1/(2L) \qquad (5)$$

This relationship does not consider factors such as electronic noise, phase problems, incorrect aperture setting, optical imperfections and mirror jitter which negatively affect the resolution claimed by mirror displacement. Imperfections of

this nature can also affect wavenumber precision and accuracy and intensity precision and accuracy.

Experimental

The output of a commercially available hollow cathode lamp (HCL) is used as the standard. An optical filter recently described (86) is used to narrow the bandpass and minimize the multiplex disadvantage. The relatively low pressure, low temperature environment of the HCL served to minimize collisional and Doppler broadening respectively, making the details of the transition visible. The Los Alamos Fourier Transform Spectrometer (64,13) is run at high resolution for this particular study. The spectra presented here is acquired at 0.026 cm^{-1} resolution with 2 scans.

Discussion

Rhenium

Spectroscopists have studied the hyperfine structure and isotope shifts of Re I (87,88,89). Re has two naturally occurring isotopes, ^{185}Re, (37.07 %) and ^{187}Re (62.93 %). Each of the two isotopes have nuclear spins greater than zero (5/2, 5/2) which led to hyperfine structure. Both have similar nuclear magnetic moments (3.172, 3.204 nuclear magnetons), respectively. The clarity and symmetry of the HFS and IS in this transition make it an excellent selection as a standard. The line profile of Re I (527.55 nm) is shown in Figure 16.

The wavenumbers for this spectrum are listed in Figure 16.

Resolution

The high resolution capabilities of an FTS can be readily tested by attempting to separate the isotope shifts for each of the hyperfine components. These isotope splittings are in the 0.06-0.07 cm^{-1} range and serve as a good standard. The splittings between the hyperfine components are in the 0.2 to 0.6 cm^{-1} range and serve as a measure for lower resolutions. The full width at half maximum (FWHM) of the individual lines in this study are 0.03-0.04 cm^{-1}.

Intensity

The intensity precision and accuracy of the Fourier transform spectrometer can be measured using the relative intensities of Re I isotopes. The ratio (37.07% : 62.93%) of the two naturally occurring isotopes serve as the standard for intensity precision and accuracy. The relative intensity (I) of the individual isotope shifts is directly related to the percent natural abundance.

$$(I_{185}/I_{187}) = (37.07\%/62.93\%) \qquad (6)$$

The isotope shifts are separated by only 0.06-0.07 cm^{-1}: therefore high resolution capabilities (< 0.05 cm^{-1}) are needed. For the hollow cathode lamp, the intensity varies 1-2% as a function of time, and so errors in this range are considered acceptable. Sources with smaller signal variations

will produce smaller errors. For the two most intense lines (18950.7397 cm^{-1}, 18950.1715 cm^{-1}) and the accompanying shifts for the less abundant isotope (18950.7994 cm^{-1}, 18950.2356 cm^{-1}), there is an acceptable systematic error of 1%. The LAFTS has a 0.1% intensity accuracy limit (13).

Wavenumber Positions

Spectroscopists routinely use Fourier Transform Spectrometers for high wavenumber precision and accuracy. Several studies (64,83,90) have taken advantage of the high wavenumber accuracy of the LAFTS. This accuracy has typically been greater than 1 part in 10^7. There are two correction factors (8) incorporated in these types of studies: a) aperture correction b) slight misalignment of instrument. They adhere to the following format:

$$\sigma' = \sigma[1 + (\Omega/4\pi) + \chi/\epsilon\ ] \qquad (7)$$

where $\Omega = \pi D^2/4F^2$ = solid angle (sr)

D = diameter of the aperture (cm)

F = focal length of collimating optics (cm)

σ = measured wavenumber (cm^{-1})

σ' = corrected wavenumber (cm^{-1})

χ = instrumental calibration (cm^{-1})

ϵ = average wavenumber (cm^{-1})

In a previous study (90), the instrumental calibration (χ) was calculated in the following manner. The emission from a uranium HCL was studied with the LAFTS. Twenty five lines were measured in the 385-395 nm range and compared against very accurate (1 part in 10^8) wavenumber values from a uranium atlas (91). With no correction factors, the values were red-shifted 0.0052 cm^{-1}. With only the aperture correction ($\Omega/4\pi$) applied, this left an average red-shift of 0.0015 cm^{-1} with a standard deviation of 0.0013 cm^{-1}. This value (0.0015 cm^{-1}) is the instrumental calibration (χ). The average wavenumber, ϵ, is simply the average of the wavenumbers being studied. For the LAFTS, the misalignment is typically smaller than the aperture correction factor. The correction factors combined are small (roughly 2.2×10^{-7}) but must be considered for high wavenumber accuracy and precision. Table 1 lists the corrected values for the Re I lines. These values are considered accurate to better than 1 part in 10^7.

Conclusion

An intensity, wavenumber, and resolution standard for Fourier Transform Spectroscopy in the visible is presented. It is chosen to evaluate the spectrometer's performance concerning resolution, intensity precision and accuracy, and wavenumber precision and accuracy. This Re I transition provides narrow, intense lines that are in an easily identifiable pattern. Re HCL's are commercially available and

easy to use in conjunction with a FTS. Obviously, many other standards could be chosen for various regions of the spectra. This standard is intense, offers symmetry in HFS and IS, and will clearly tell if the FTS is performing up to claimed specifications.

Figure 16. Re I line profile clearly shows hyperfine structure (HFS) and isotope shifts (IS). The corrected wavenumbers for Re I (18950 cm^{-1}) transition are: 18950.8035 (^{185}Re), 18950.7438 (^{187}Re), 18950.2397 (^{185}Re), 18950.1756 (^{187}Re), 18949.8044 (^{185}Re), 18949.7384 (^{187}Re), 18949.4877 (^{185}Re), 18949.4189 (^{187}Re), 18949.3484 (^{185}Re), 18949.2811 (^{187}Re).

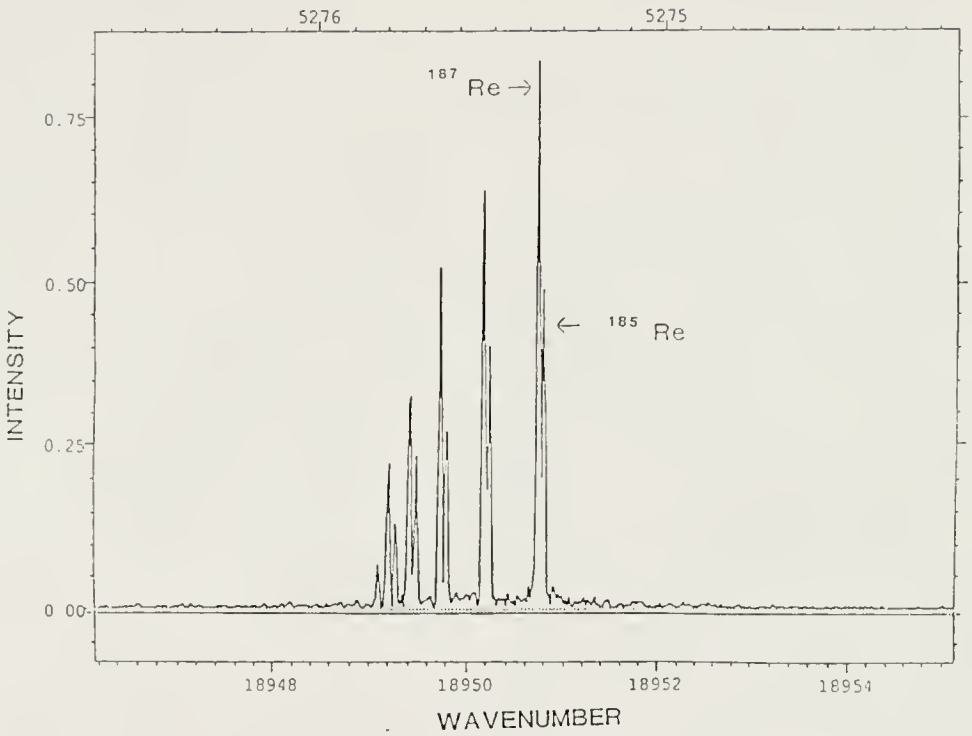
5276
5275
^{187} Re →
← ^{185} Re
0.75
0.50
0.25
0 00
INTENSITY
18948
18950
18952
18954
WAVENUMBER

CHAPTER 8
UNDERSTANDING NOISE IN FOURIER TRANSFORM SPECTROSCOPY

Introduction

Various aspects of noise studies in Fourier Transform Spectroscopy have been reviewed by in several books, including Griffths and deHasth (92), Chamberlain (93), Bell (94), and Bracewell (95). Theoretical modeling and experimental work involving noise in FT-UV/VIS consist of work by Horlick and coworkers (1,4,96), research at Imperial College (97-99), work by Jim Brault of Kitt Peak National Observatory (100,101), Voigtman and Winefordner (102), Hirschfeld (103-105), Faires (2,106,107), Sakai and Murphy (107), Natale and Ventura (108), Knacke (109), Luc and Gerstenkorn (110), and Emonds dissertation from the Orsay (France) FT facility (111). A complete survey of the literature would envelope many more papers on various aspects of FTS.

In this paper, a simple system that crudely mimics a Michelson Interferometer analyzing monochromatic and dichromatic light for noise studies is described. It is critical to understand and characterize noise sources in ultraviolet and visible FTS, whether they be flicker (1/f), white noise, or interference noise (60 Hz, etc), if they are to be minimized or eliminated. In infrared FTS (FT-IR), the

system is typically detector noise limited. In FT-UV/VIS, the detectors (typically photomultiplier tubes or Si-PIN diodes) are not the limiting noise source. Commonly used sources in atomic emission spectroscopy such as flames, plasmas, and discharges, are source noise limited. For a FTS to show a SNR gain over a dispersive type system, the FT experiment would have to be operating near or at the detector noise. If shot or flicker noises are limiting, the SNR comparison becomes complex.

In this system, the noise characteristics of any light source can be studied. Chopping the source at some frequency, f_i (Hz), equals the rate of constructive and destructive interference, R_i (Hz), which is related to the wavelength studied (λ_i, cm) and the mirror velocity (v_i, cm/s) by the relationship

$$f_i = R_i = v_i/\lambda_i \qquad (8)$$

The same detector used in the FTS can be retained. Chopping at a set frequency allows us to study the magnitude and type of noise in that region. The effects of low frequency noises (eg. 1/f, 60 Hz) wrapping around the desired line profile, external sources producing interferences, etc. can be characterized. For example, a Cu vapor laser used in our lab fires at 6 kHz. This produces a strong signal at 6 kHz and its respective harmonics (12, 18, 24, kHz, etc.). Research

buildings typically produce a wide range of interference noises that can be misidentified if not correctly identified.

Experimental

The experimental setup used in this study is shown in Figure 17. A Na (589.0 nm) HCL and a Helium Neon laser are the sources employed for demonstration purposes. The setup has been used in conjunction with many sources, including HCL's, diode lasers, and various white light sources. Figure 17 shows the laser light split and the geometric arrangement which produces frequencies corresponding to different wavelength's in a Michelson. A photomultiplier tube (1P28, -760 V) is the detector.

Neutral density filters are used as needed to attenuate the light flux entering the monochromator. The beam splitters and mirrors used are optimized for the far visible and near infrared studies. Mechanical choppers employed here have maximum chopping rates of 680 and 1100 Hz. Because mirror velocities for a typical Michelson interferometer range from 0.01 to 4 cm/s, the wavelength range considered (near IR, visible, UV) and reasonable mirror velocities (v_1), the maximum rates of constructive and destructive interference (R_1, 680 and 1100 Hz) are slow but possible. An extreme range for FT-UV/VIS/NIR modulation rates is 100 HZ (1000nm, 0.01 cm/s) to 200,000 Hz (200 nm, 4 cm/s) with 400-20,000 Hz being reasonable.

The 0.25 m monochromator was used to minimize/eliminate the effects of unwanted light. The output of the PMT was sent to a Wavetek 5820B Cross Channel Spectrum Analyzer. This data processor uses a Fast Fourier Transform (FFT) and displays the resulting Noise Power Spectra in $dBV/(Hz)^{1/2}$ (x-axis) verses Hz (y-axis). The Wavetek has a maximum bandwidth of 50 kHz (0-50 kHz). 64 scans were coadded for all spectra presented.

Results

Figure 18a shows the transform of the PMT dark current (no light striking it). For UV/VIS/NIR FTS the region of interest lies in the 500-20000 Hz range. The exact origin of the noises at approximately 14 and 41 kHz are not known but appear to be from an external (not PMT) source. The PMT voltage was varied from 400-800 V, but the magnitude of the noises (14, 41 kHz) remained constant. Figure 18b shows the noise power spectra of the PMT output of unchopped Na HCL (589.0 nm) emission. It is important to notice the magnitude of the y-axis ($dBV/(Hz)^{1/2}$) in relationship to 18a. The noise level has been raised substantially. Noise spikes at 14 and 41 kHz that were prominent in 18a are less significant because of the rising background. Two flicker noise components are obvious. The low frequency (0-10 Hz) flicker noise component is in the 0-10 Hz region. The higher frequency flicker noise component decreases at a slower rate from 0 Hz to 50 kHz, the upper frequency limit of the Wavetek instrument. The drop

off of the high frequency component is not as dramatic as the low frequency (0-10 Hz) component but can be precisely measured. Figure 18c shows the HCL emission with sand passing between the HCL and monochromator (see figure 17). This has been described as a reliable method to generate a strong 1/f component on a light source. The increase in NPS is especially high in the 0-10 kHz range. Recalling that most Michelson's operating in the UV/VIS have constructive and destructive interference rates in 400-10,000 Hz range, a source with a large flicker noise component, such as a flame or atmospheric plasma, will make achieving a detector shot noise or a photon shot noise limited case impossible. Figures 18a,b, and c are studies of the noise characteristics of the PMT that address baseline noises and not the modulated signal.

Figure 19a and b is the measured output of a Na HCL (589.0 nm) chopped at 680 Hz. The experimental design shown in figure was utilized with one of the arms blocked so no light could pass. The bandpass is 0-1 kHz. Decreasing the frequency range increases the resolution. Figure 19a shows the modulated HCL emission line. In 19b, sand is used to generate a flicker noise component on the modulated HCL emission. This raises the low frequency (0-10 Hz) (1/f) and the high frequency (0-50 kHz) (1/f) noise magnitudes. In figure 3a,b, and c the 1/f noise from a HCL decreases from 0-50 kHz was demonstrated. The important point in 19a and b is that the system is flicker noise limited but may be perceived

as being shot noise limited if a large frequency range is not examined. The slope of the flicker component is not dramatic enough to be detected in a small bandpass (eg. 0.5-1 kHz). A larger frequency range (0-50 kHz, or greater) must be analyzed to determine if the flicker noise component is limiting. The background in a narrow frequency range may appear to be a uniform background that is interpreted to be shot noise limited.

Figure 20a shows the NPS of the He-Ne laser emission modulated at 680 Hz with the laser light passing through the second chopper blocked. Figure 20b shows the same modulated line (680 Hz) with a 830 Hz signal of equal magnitude also striking the detector. The average baseline increases (70 $dBV/(Hz)^{1/2}$ to 60 $dBV/(Hz)^{1/2}$) while the signal magnitude remains constant. The He-Ne laser has a 1/f component that is still decreasing at 50 kHz (upper limit of this system). The increase in baseline in this situation can be attributed to an increase in both the shot and flicker noise caused by the addition of the second (830 Hz) frequency.

Conclusion

A system that allows one to study the affect of noises in a Michelson interferometer is outlined. The characterization of noise possible in a UV/VIS FTS can be made without using a Michelson interferometer. Some commercially available interferometers suffer from phase problems, mirror jitter,

electronic noise, etc. Problems of this nature, depending on their severity, can negatively affect the quality of spectra obtained by the instrument giving false impressions as to the true potential of the technique. Problems of this nature do not allow one to study the true effect of source flicker noise on the spectra or achieve a shot noise limited case.

Flicker (1/f) noise is shown to have two components in HCL emission. The low frequency 0-10 Hz component and the higher frequency, lower magnitude component that steadily decreases out to at least 50 kHz. This high frequency (1/f) component must be measured and considered if a shot noise limited case is being claimed. Sources tested (He-Ne laser, white light sources, other HCL's) had similar NPS; that is the high frequency flicker component was still decreasing at 50 kHz. Using a spectrum analyzer with a bandwidth extending into the MHz region would allow the extend of the high frequency flicker component to be evaluated.

Figure 17. The emission of a He-Ne laser is split, in equal magnitudes, chopped at different frequencies, recombined, and analyzed. Numerous other light sources such as a HCL, white light, and diode laser, have been studied with this design.

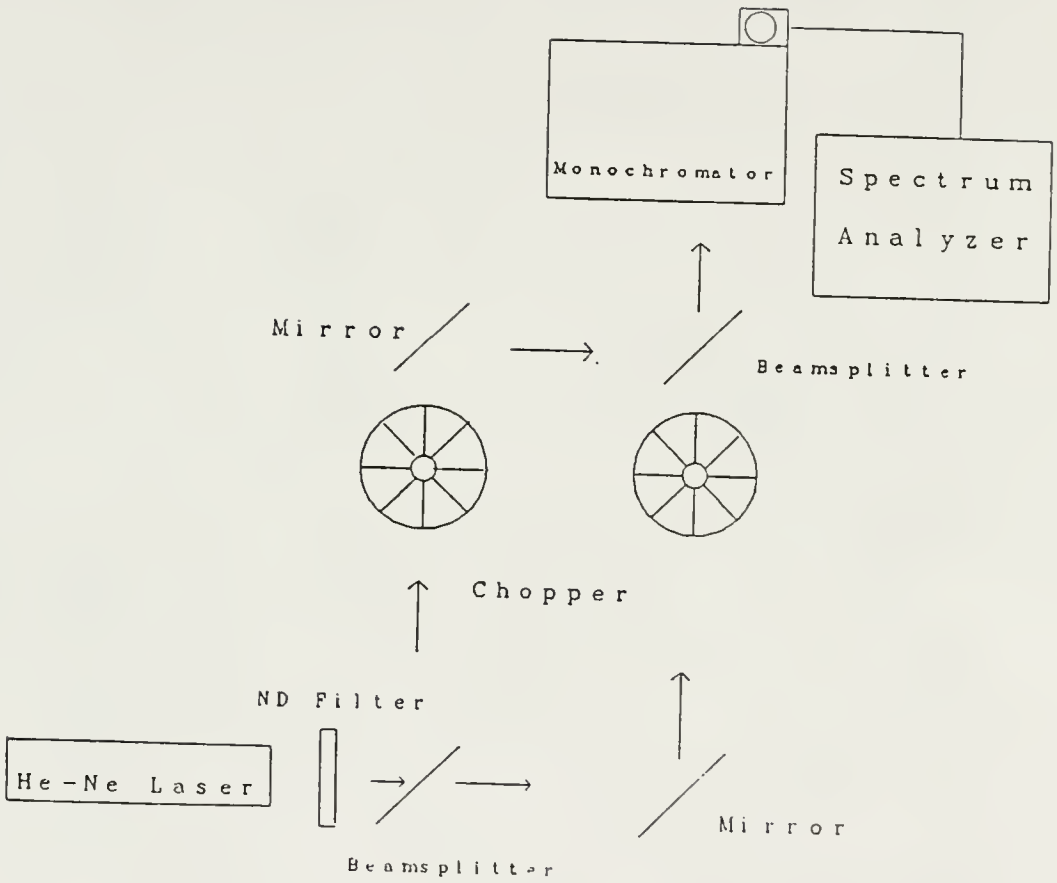
Monochromator
Spectrum Analyzer
Mirror
Beamsplitter
Chopper
ND Filter
He-Ne Laser
Mirror
Beamsplitter

Figure 18. Noise power spectra of phphotomultiplier tube (PMT) under various conditions of operation.
(a, top) The noise power spectra (NPS) of the dark current and interferences picked up by the PMT.
(b, middle) The noise power spectra (NPS) of unchopped Na HCL emission striking the PMT.
(c,bottom) The NPS of Na HCL emission with strong flicker component induced by passing sand through the light path.

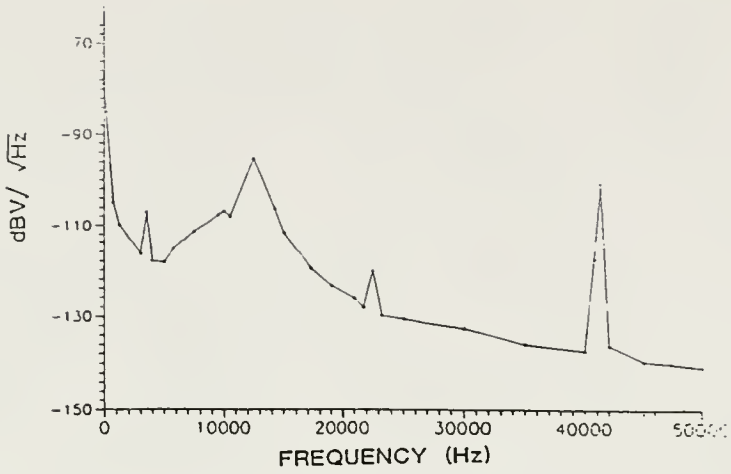
dBV/ √Hz
-70
-90
-110
-130
-150
0
10000
20000
30000
40000
FREQUENCY (Hz)

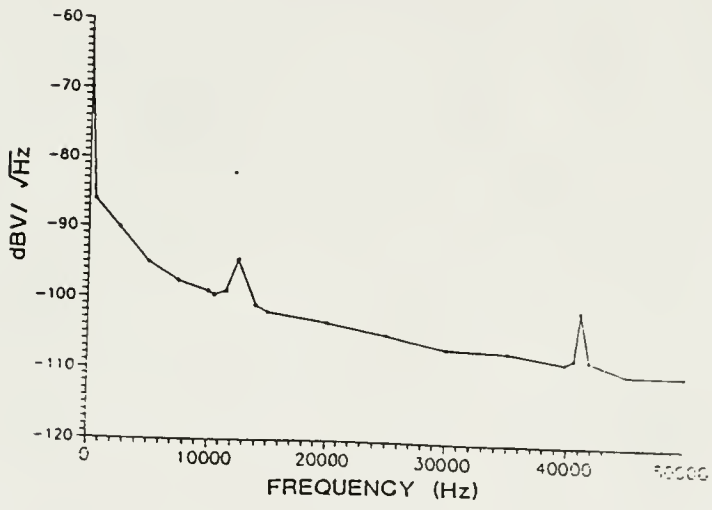
dBV/ √Hz
-60
-70
-80
-90
-100
-110
-120
0
10000
20000
30000
40000
FREQUENCY (Hz)

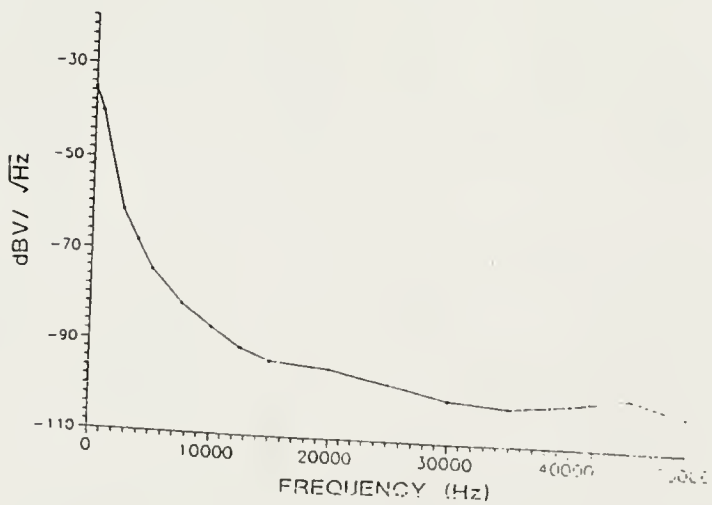
dBV/ √Hz
-30
-50
-70
-90
-110
0
10000
20000
30000
40000
FREQUENCY (Hz)

Figure 19. Modulated signal of sodium (Na) HCL striking PMT is transformed revealing its noise power spectra.
(a, top). Na HCL emission modulated at 680 Hz.
(b, bottom) Na HCL emission modulated at 680 Hz with flicker component induced by sand. Due to small frequency range, flicker noise may be interpreted as shot noise.

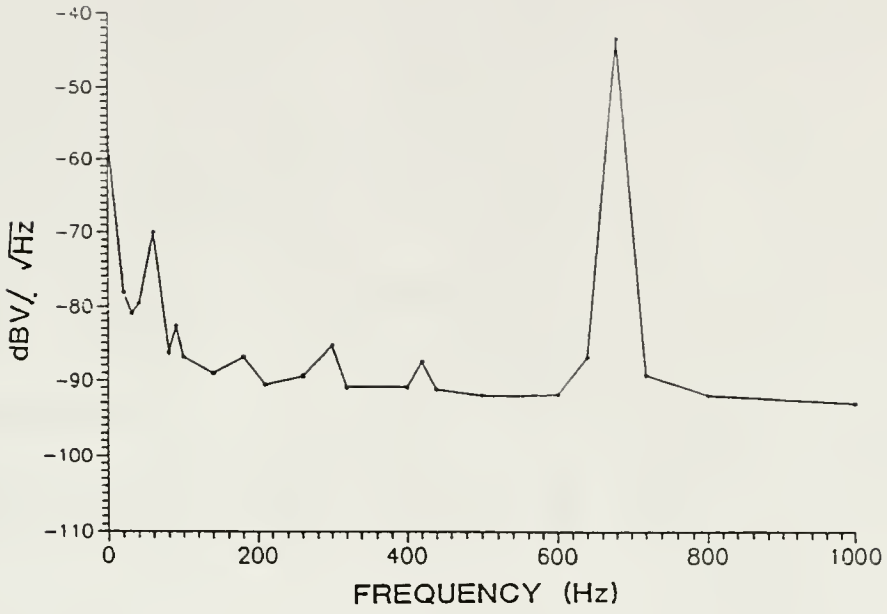
-40
-50
-60
-70
-80
-90
-100
-110
dBV/ √Hz
0
200
400
600
800
1000
FREQUENCY (Hz)

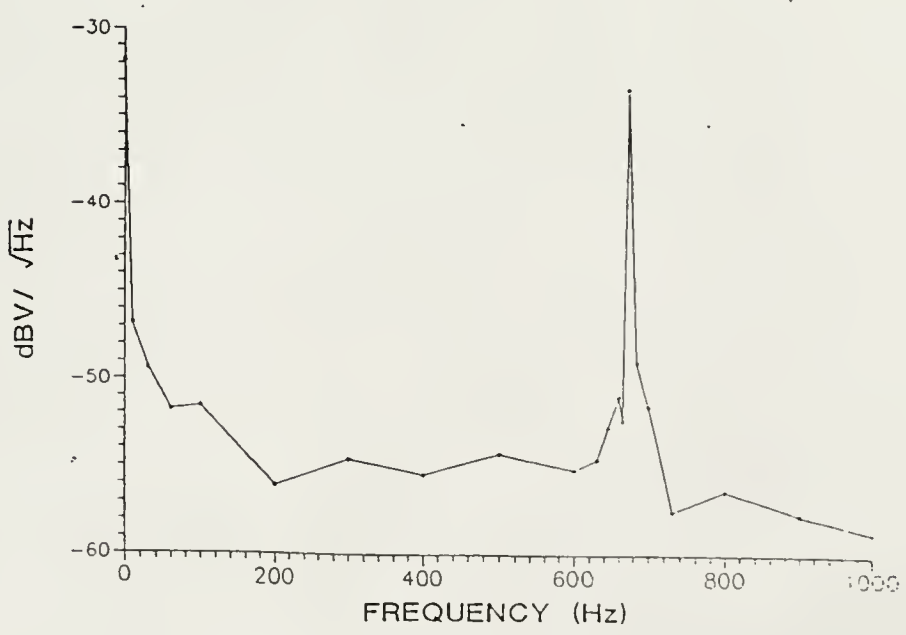
-30
-40
-50
-60
dBV/ √Hz
0
200
400
600
800
1000
FREQUENCY (Hz)

Figure 20. Modulated He-Ne laser signal is transformed revealing its noise power spectra.
(a,top) The modulated (680 Hz) signal of He-Ne laser.
(b, bottom) The same modulated line but an additional line (830 Hz, not shown) of equal magnitude is striking the detector increasing the baseline noise. The increase is attributed to a combination of flicker and shot noises.

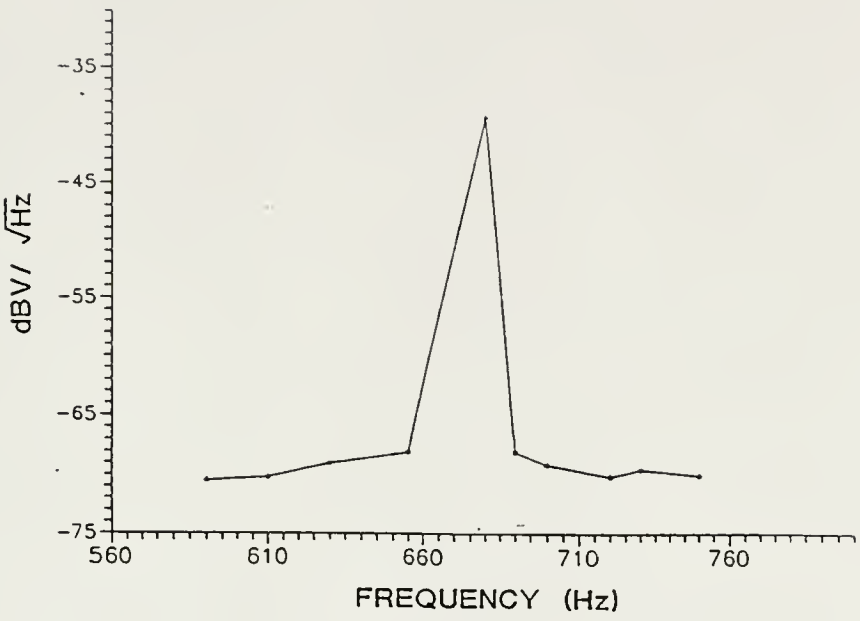
-35
-45
-55
-65
-75
dBV/ √Hz
560
610
660
710
760
FREQUENCY (Hz)

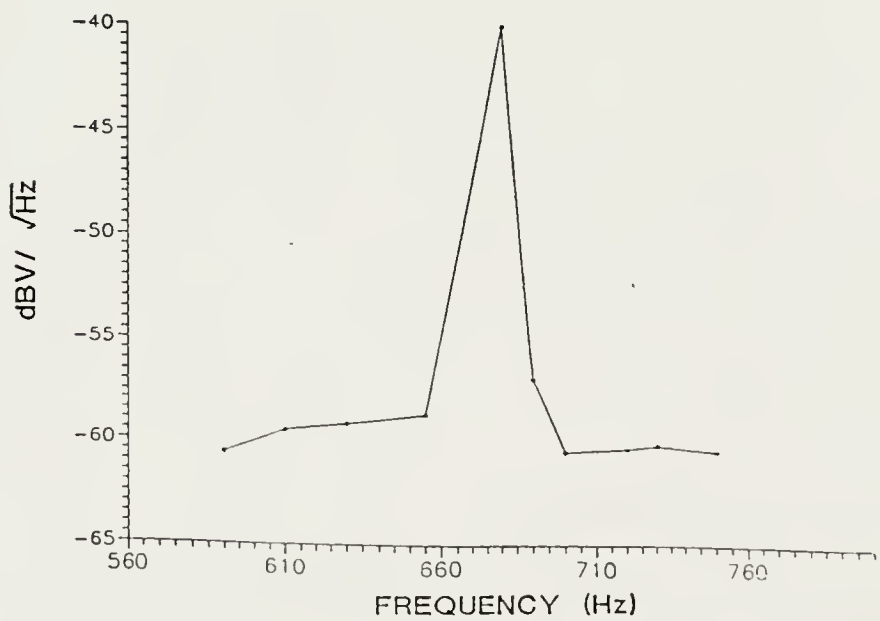
-40
-45
-50
-55
-60
-65
dBV/ √Hz
560
610
660
710
760
FREQUENCY (Hz)

CHAPTER 9
RESOLUTION AND SIGNAL TO NOISE RATIOS IN FOURIER TRANSFORM SPECTROSCOPY

Hobbs et al. (97) discussed the effect of resolution on the signal to noise ratio (SNR) in atomic emission (ICP) experiments. Data concerning the SNR versus resolution were not presented in a paper primarily concerned with source noise in the ICP and its effects on the FT spectra. To briefly review Hobbs et al. (97, p. 543), "There is actually an apparent gain of $(n)^{1/2}$ in going to higher resolution. This gain has in fact been earned by increasing the integration time" (n is the number of spectral data points acquired and can be directly related to integration time provided other factors such as mirror velocity and data acquisition rate are constant). This is true if the signal constitutes the integrated area for the emission line profile being studied. The signal is conserved but will be broadened and with a decreased in intensity by instrumental effects at poor resolutions.

Many analytical spectroscopists use the basic relationship S/N = (average signal amplitude) /(average noise amplitude) for SNR calculations in Fourier Transform Spectroscopy (FTS). In FTS, the signal (line profile) can be

"smeared out" or instrumentally broadened at low resolutions decreasing the signal amplitude (peak height) but not the integrated area of the signal.

In this note, the nonlinear gain in SNR with resolution is demonstrated with a Cu HCL (515.32 nm) emission line, at five resolutions (2, 0.7, 0.2, 0.07, 0.02 cm^{-1}) using a signal amplitude calculation for the SNR. The Los Alamos Fourier Transform Spectrometer (13,64) (LAFTS) was utilized to acquired the data. Table 12 presents data (resolution, SNR, number of points, etc.) for Cu HCL 515.32 nm emission line, respectively, at five resolutions (2, 0.7, 0.2, 0.07, 0.02 cm^{-1}) with the same mirror velocity. The signal-to-noise ratio's were normalized so all resolutions have identical integration times. The method to calculate signal to noise ratio's shown in Table 12 is a signal amplitude to noise amplitude ratio. The best resolution, 0.02 cm^{-1}, is the physically resolved line profile.

Figure 21 shows the effects resolution has on the same Cu HCL emission line at three resolutions (2, 0.2, 0.02 cm^{-1}). Data in table 12 shows that the line profile is significantly broadened (FWHM increases) at lower resolutions and the signal intensity (interpreted from decreasing SNR with a constant noise level) decreases. The SNR for all resolutions should be the same since the integration times are identical and other parameters (eg. mirror velocity, aperture, HCL current, etc.) are held constant. This is not the case. Comparing the SNR

values for 0.02 cm^{-1} to 2 cm^{-1} resolutions, 1321 vs 31, respectively, it is obvious that the instrumental broadening and subsequent decrease in signal amplitude intensity causes a substantial decrease in SNR. For the same SNR to be achieved for all resolutions, a hypothetical situation such as the following would have to be achieved.

Assume we are working at the shot noise limit using a monochromatic source, data is acquired at two resolutions (0.02 and 2 cm^{-1}; where 0.02 cm^{-1} is physically resolved) with equal integration times (eg. 0.02 cm^{-1}, 1 scan; 2 cm^{-1}, 100 scans). There is a well defined free spectral range (eg. 10,000 cm^{-1}). At 0.02 cm^{-1} the line profile can be described with a Gaussian function, and at 2.00 cm^{-1} the line profile can be described by the instrumental function. Integrating both functions over the free spectral range will give essentially the same integrated signal magnitude. Integrating the noise over the FSR will also be equal for both resolutions. The noise per resolution element will be higher at low resolution but the total noise will remain equal. The energy (light flux) striking the detector is conserved irrelevant of mirror displacement. Measuring signal and noise magnitudes in this manner is, of course, not practical for most analytical spectroscopists but it shows that signal and noise integrated magnitudes remain constant for all resolutions with equal integration times.

Hobbs et al. (97, p. 544) pointed out "Although the

signal to noise ratio for an emission spectrum, when properly evaluated, is independent of resolution until the lines are actually resolved, there is a real gain to be made in the line to continuum ratio." These data presented here support their statement and demonstrate the misinterpretation possible. When using a ratio method for an SNR determination at low resolutions, there is a dependence of SNR on resolution even when integration times are equal. If an analytical determination of FT-UV/VIS is to be made using relative intensities, it should be carried out at high resolution (physically resolved) to maximized signal intensity. We point out his possible error because several analytical evaluations of FT-UV/VIS have been carried out at poor resolutions using a ratio of intensity height to noise for SNR determination.

Figure 21. Cu (515.32 nm) emission from a HCL at three (0.02 cm^{-1} (top), 0.2 cm^{-1} (middle), 2 cm^{-1}(bottom)) resolutions. Using poorer resolutions causes the loss of all physical information involving HFS and IS, as well as a true physical line width. The top x-axis is in angstroms and the bottom is in wavenumbers (cm^{-1}).

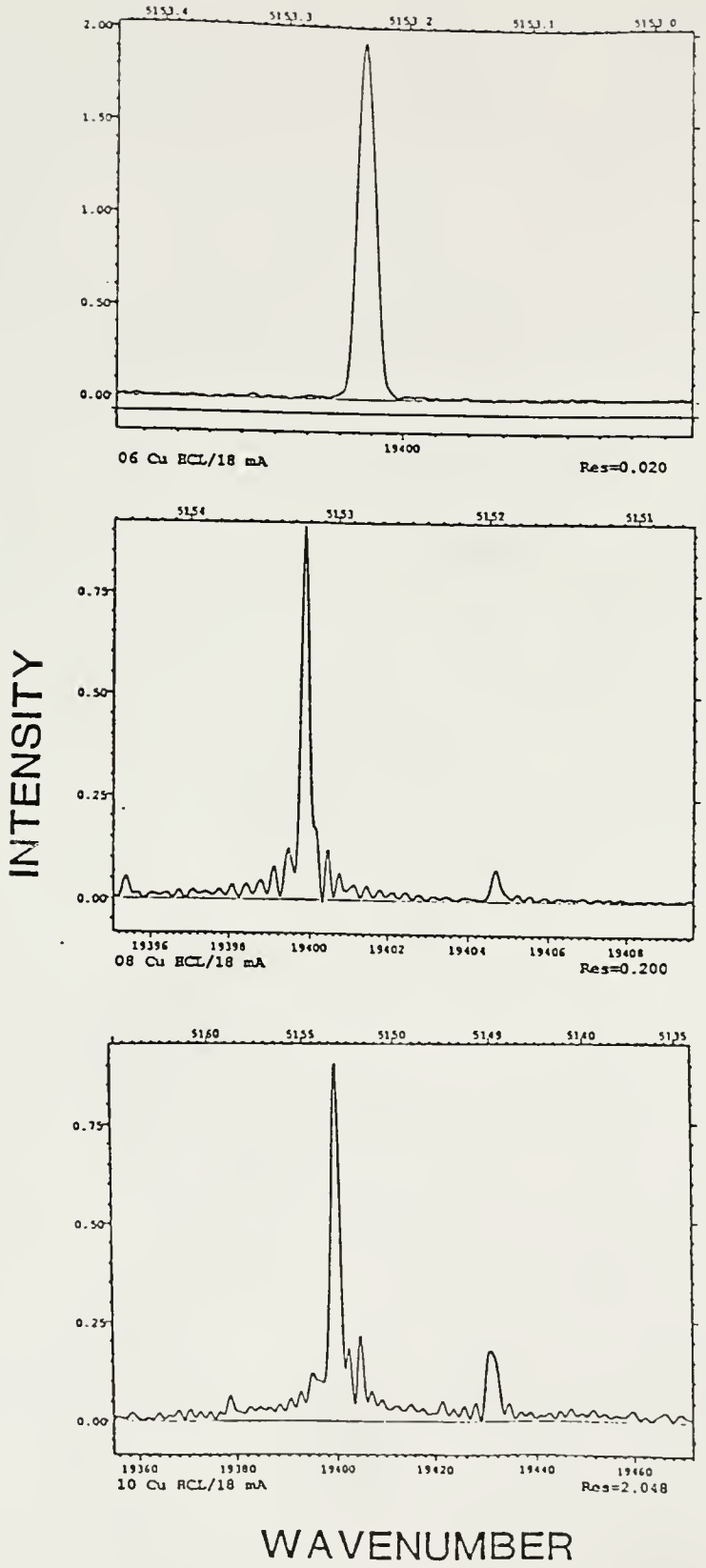
INTENSITY
WAVENUMBER
06 Cu ECL/18 mA
Res=0.020
08 Cu ECL/18 mA
Res=0.200
10 Cu ECL/18 mA
Res=2.048

Table 12. Figures of Merit for Cu (515.32 nm) line from a Hollow Cathode Lamp measured by the LAFTS.

RESOLUTION cm^{-1}	0.02	0.07	0.2	0.7	2.0
NUMBER OF POINTS (N)	$3.8x10^6$	$8.6x10^5$	$3.0x10^5$	$8.5x10^4$	$2.9x10^4$
FSR, cm^{-1}	33357.27	30011.0	30011.0	30011.0	30011.0
SNR	1321.4	1263.6	765.9	207.1	31.3
FWHM, cm^{-1}	0.0714	0.190	0.25	1.00	3.87
N/cm^{-1}	114	28.5	9.98	2.84	0.998
N/FWHM	8.14	5.41	2.49	2.84	3.86

CHAPTER 10
CONCLUSIONS

A common misnomer among analytical spectroscopists is that Fourier Transform Spectroscopy in the ultraviolet and visible does not work. For over a decade, the Fourier Transform Spectrometer at Kitt Peak National Observatory (Arizona) has been routinely taking excellent data in uv/vis for physicists and astronomers. The Los Alamos Fourier Transform Spectrometer can operate at higher resolution and higher wavenumber accuracy than its predecessors. During my tenure at the Los Alamos Fourier Transform Spectrometer, my work resulted in the first publication from the LAFTS (64), first patent (70), and the last experimental work (83) to be carried out and published on the instrument. During its operation I was the primary user of this national facility. The Department of Energy spent an estimated 13 million dollars to build the instrument. Once the instrument was built and operational, the DOE decided not to fund it anymore. Outside funding could not be secured, so the instrument now sits in mothballs with no future ahead of it. To even the most casual of observers, it is a tremendous waste of financial resources and brain power. Its full potential had been achieved but was not allowed to be exploited. The LAFTS would have supplied a

steady stream of spectroscopic data for scientists worldwide to use.

Fourier Transform Spectroscopy in the ultraviolet and visible does work. The ability to exactly measure wavenumber positions, resolve isotope shifts and collect a large free spectral is readily demonstrated in this dissertation. Using a MacIntosh computer allowed us to process 4 million point Fast Fourier Transforms in 30 to 40 minutes. As time goes on, the computation time will become faster. Advances in the optics industry brought about by major projects such as the Hubble Space Telescope, will increase the quality and decrease the costs of optics routinely available to spectroscopists at a reasonable costs. The ability to accurately move the mirror should also advance with technology. I have recently had contact with Kitt Peak, NIST (Chelsea Instrument) and Imperial College (Chelsea FTS creator) about future work. This work will be aimed at supplying data fundamental to plasma spectroscopy. Work on hyperfine structures and isotope shifts of metals as well as more detailed work on line shifts is planned.

REFERENCES

(1) Horlick, G.; Yuen K.; Anal. Chem., 47, 775A (1975).

(2) Faires, L.; Anal. Chem. 58, 1023A (1986).

(3) Thorn, A.; J. Anal. Atom. Spectrom., 2, 227 (1987).

(4) Stubley, E.A.; Horlick, G.; Appl. Spectrosc. 39, 800 (1985).

(5) Stubley, E.A.; Horlick, G.; Appl. Spectrosc. 39, 805 (1985).

(6) Stubley, E.A.; Horlick, G.; Appl. Spectrosc. 39, 811 (1985).

(7) Marra, S.; Horlick, G.; Appl. Spectrosc. 40, 804 (1986).

(8) Faires, L.M.; Fourier Transform and Polychromator Studies of the Inductively Coupled Plasma, PhD. Thesis, University of New Mexico, Los Alamos-9888-T (1985).

(9) Faires, L.M.; Spectrochim. Acta. 40B, 1473 (1985).

(10) Faires, L.; Palmer, B.; Engleman, R.; Niemczyk, T.; Spectrochim. Acta, 40B, 545 (1985).

(11) Faires, L.; Palmer, B.; Brault, J.; Spectrochim. Acta, 40B, 135 (1985).

(12) Palmer, B.A.; Los Alamos Technical Bulletin 576-111/10060, The Los Alamos Fourier Transform Spectrometer, LALP-85-16 (1985).

(13) Parsons, M.L.; Palmer, B.; Spectrochim. Acta, 43B, 75 (1988).

(14) Belchamber, R.M.; Horlick, G.; Spectrochim. Acta, 37B, 17 (1982).

(15) Salin, E.D.; Horlick, G.; Anal. Chem., 52, 1578 (1980).

(16) Walden, G.; Bower, J; Nikdel, S.; Bolton, D.; Winefordner J.D.; Spectrochim. Acta, 35B, 535 (1980).

(17) Benetti,P.; Bonelli, A.; Cambiaghi, M.; Frigieri, P.; Spectrochima Acta, 37B, 1047 (1982).

(18) Duursma, R.; Smit, H.; Maessen, F.; Analytica Chimica Acta, 133, 393 (1981).

(19) Abdallah, M.; Mermet,J.; Spectrochim. Acta, 37B, 391 (1982).

(20) Abdallah, M.; Abdelrahman,A.; Eid, M.; Indian Journal of Pure and Applied Physics. 22, 458 (1984).

(21) Wolnick,K; Miller,D; Seliskar,C.; Fricke,F.; Appl. Spectrosc., 39, 930 (1985).

(22) Seliskar, C.; Warner, D.; Appl. Spectrosc. 39, 181 (1985).

(23) Miller, D.; Seliskar, C.; Davidson, T.; Appl. Spectrosc. 39, 13 (1985).

(24) Fleitz, P.; Seliskar, C., Appl. Spectrosc. 41, 679 (1987).

(25) Chan, S.; Van Hoven, R.; Montaser, A.; Anal. Chem., 58, 2342 (1986).

(26) Chan, S.; Montaser, A.; Spectrochim. Acta, 40B, 1467 (1985).

(27) Chan, S.; Montaser, A.; Appl. Spectrosc., 41, 545 (1987).

(28) Montaser, A.; Van Hoven, R.; CRC Critical Reviews in Analytical Chemistry, 18, 45 (1987).

(29) Tan, H; Chan, S.; Montaser, A.; Anal. Chem., 60, 2542 (1988).

(30) Coster, D.; Brons, H.; Z. Phys., 84, 304 (1933).

(31) Hasegawa, T.; Winefordner, J.D.; Spectrochim. Acta, 42B, 637 (1987).

(32) Seliskar, C.; Miller, D.; Fleitz, P.; Appl. Spectrosc., 41, 658 (1987).

(33) Tomasik, Z.; Zyrnicki, W.; Spectrosc. Lett., 19, 179 (1986).

(34) Porter R.; Harshbarger, W., J. Electrochem., 126, 460-464 (1979).

(35) Abdallah, M.; Mermet, J.; J. Quant. Spectrosc. and Radiat. Transfer, 19, 83-91 (1978).

(36) Cramarossa, F.; Benedictis, S.; Ferraro, G.; J. Quant. Spectrosc. and Radiat. Transfer, 23, 291-301 (1980).

(37) Bechtel, J.; Appl. Optics, 18, 2100-2106 (1979).

(38) Zeeman, P.; Terblanche, S.; Visser, K.; Hamm, F.; Appl. Spectrosc., 32, 572-576 (1978).

(39) Cabannes, F.; Pure Appl. Chem., 39, 381 (1974).

(40) Czernichowski, A.; J. Phys. D., 20(5), 559-564 (1987).

(41) Gudeman, C.; Martner, C.; Saykally, R.; Chem. Phys. Lett., 122, 108-112 (1985).

(42) Bailly, D.; Rossetti, C.; Guelachvili, G.; Chem. Phys., 100, 101-118 (1985).

(43) Golubovskii, Y.; Telezhko, V.; J. Appl. Spectrosc., 39, 999-1003 (1983).

(44) Plain, A.; Ricard, A.; Phys. Lett. A, 95A, 235-238 (1983).

(45) Zyrnicki, W.; Tomasik, Z.; Nowicka, I.; Spectrosc. Lett., 17(3), 207-217 (1984).

(46) Davis, G.; Gottscho, R.; J. Appl. Phys. 54(6), 3080-3086 (1983).

(47) Zheng, J.; Snow, J.; Murphy, D.; Leipertz, A.; Chang, R.; Farrow, R.; Opt. Lett., 9(8), 341-343 (1984).

(48) Burlbaw, E.; Armstrong, R.; Appl. Opt., 22(18), 2860-2863 (1983).

(49) Lapp, M.; Goldman, L.; C.Penney, C.; Science, 175 (4026), 1112-1115 (1972).

(50) Barrett, J.; Harvey, A.; J. Opt. Soc. Amer., 65, 392-398 (1975).

(51) Gottscho, R.; Field, R.; Dick, K.; Benesch, W.; J. Mol. Spectrosc., 74, 435-438 (1979).

(52) Herzberg, G.; Molecular Spectra and Molecular Structure, (Diatomics) D. van Nostrand, Princeton (1950).

(53) Michel, H.; Gantois, M.; 18th Int. Conf. on Heat Treatment of Materials, (conference proceedings) Detroit (1980).

(54) Baronnet, J.; et al., I.S.P.C.4, Zurich, 341 (1979).

(55) Svindon, A.; Sobolev, N.; Tselikov, G.; Zh. Eksp. Teor. Fiz. Pis'ma, 6, 542 (1967).

(56) Dieke, G.H.; Crosswhite, H.M.;J. Quant. Spectrosc. Radiat. Transfer, 2, 97-197 (1962).

(57) Klim, M.; Nikdel, S.; Spectroscopy, 2, 57 (1987).

(58) Schleicher, R.; Barnes, R.; Anal. Chem., 47, 724-728 (1975).

(59) Allemand, C.; Barnes, R.; Spectrochim. Acta, 33B, 513-534 (1978).

(60) Thorn, A.P., Spectrophysics, Chapman & Hall, London, 1974 (p. 377).

(61) Kornblum, G.; de Galen, L.; Spectrochim. Acta, 32B, 71-96 (1977).

(62) Manning, T.; Bentley, G.; Palmer, B.; Hof, D., Spect. Lett., 3, 341-344 (1989).

(63) Walters, P.; Chester, T.; Winefordner, J.; Appl. Spectros., 31, 1 (1977).

(64) Manning, T.; Palmer, B.; Hof, D.; Anal. Chem., 1052-1056 (1989).

(65) Huddlestone R.H., Leonard S.L., Plasma Diagnostic Techniques, Academic Press, New York (1965).

(66) Matsummoto, S.; Hino, M.; Kobayashi, T.; Appl. Phys. Lett., 51(10), 737-739 (1987).

(67) Downey, S.; Nogare, N.; Appl. Spectros., 38, 876-79 (1984).

(68) Montaser, A.; Golightly, D.W.; Inductively Coupled Plasmas in Analytical Atomic Spectrometery, VCH Publishers, Inc., Federal Republic of Germany (1987).

(69) Eckert, H.; Spectrochim. Acta, 33B, 591-608 (1978).

(70) Manning, T.; Palmer, B.; Hof, D.; Department of Energy patent docket S-68,054 (1988)

(71) Alkemade, C.Th.J.; Hollander, Tj.; Snelleman, W; Zeegers, P.J.Th.; Metal Vapors in Flames. Pergamon Press, Oxford (1982).

(72) Griem, H.R.; Plasma Spectroscopy. McGraw-Hill, New York, (1964).

(73) Breene, R.G.; The Shift and Shape of Spectral Lines. Pergamon, Oxford-New York (1961).

(74) Konjevic, N.; and Weise, W.L.; J.Phys. Chem. Ref. Data 5, 259 (1976).

(75) Konjevic N.; Roberts, J.; J. Phys. Chem. Ref. Data 5, 209 (1976).

(76) Whaling, W.; Brault, J.W.; Physica Scripta, 38, 707 (1988).

(77) Kuhn, H.G.; Atomic Spectra, 2 ed., Longmans, London (1969).

(78) Kato, K.; Fukushima, H.; Nakajima, T.; Spectrochim. Acta, 39b, 979 (1984).

(79) Boumanns, P.W.J.M.; Vrakking, J.J.A.M.; Spectrochim. Acta 39B, 1239 (1984).

(80) Li, H.H.; Humphreys, C.J.; J. Opt. Soc. Am. 64, 1072 (1974).

(81) Fuhr, J.R.; Martin, G.A.; and Wiese, W.L.; Atomic Transition Probabilities: Iron through Nickel, J. Phys. Chem. Ref. Data 17, Supplement 4 (1988).

(82) Voigtman, E.; Winefordner, J.D.; Appl. Spectrosc., 41, 1182 (1987).

(83) Manning, T.J.; Winefordner, J.D.; Palmer, B.A.; Hof, D.E.; Spectrochim. Acta B, (in press)

(84) Hirschfeld, T.; Chase, B.; Appl. Spectrosc., 40, 133 (1986).

(85) Hirschfeld, T.; Milanovich, F.; Microbeam Analysis, D. Newbury, Ed., F.J. Heinrich, San Francisco, (1982) p. 270.

(86) Manning, T.J.; Winefordner, J.D.; Rev. Sci. Instr., 61(5), 1554 (1990).

(87) Kropp, J.R.; Kronfeldt, H.D.; Lucas, A.; Winkler, R.; Physica 138C, 335 (1986).

(88) Hohberg, G.; Krebs, K.; Schulz, B.; and Winkler, R.; Z. Phys. 186, 380 (1965).

(89) Burger, K.; Burghardt, B.; Buttgenbach, S.; Harzer, R.; Hoeffgen, H.; Meisel, G.; Traber, F.; Z. Phys. A307, 201 (1982).

(90) Manning, T.J.; Winefordner, J.D.; Palmer, B.; J. Quant. Spec. Rad. Trans., (in press)

(91) Palmer, B.A.; Keller, R.A.; Engleman, R.; An Atlas of Uranium Emission Intensities in a Hollow Cathode Discharge, (Los Alamos Report) LA-8251-MS (1980).

(92) Griffiths, P.; deHaseth, J.; Fourier Transform Infrared Spectrometery, John Wiley and Sons, New York, (1986).

(93) Chamberlain, J.; The Principles of Interferometeric Spectroscopy, John Wiley and Sons, New York (1972).

(94) Bell, R.J.; Introductory Fourier Transform Spectroscopy, Academic Press, New York (1972).

(95) Bracewell, R.; The Fourier Transform and its Applications, McGraw-Hill, New York (1965).

(96) Ng, Y.; Horlick, G.; Appl. Spectrosc., 39, 834-841 (1985).

(97) Hobbs, P.; Spillane, D.E.; Snook, R.D.; Thorne, A.P.; J.Anal. Atom. Spectrosc., 3, 543 (1988).

(98) Thorne, A.; J. Anal. Atom. Spectrom., 2, 227 (1987).

(99) Irfan, A.Y.; Thorne, A.P.; Bohlander, R.A.; Gebbie, H.A.; J.Phys. E: Sci. Instrum., 6, 12 (1979).

(100) Brault, J.W.; Phil. Trans. R.Soc.Lond. A 307, 503-511 (1982).

(101) Brault, J.W.; J.Opt.Soc.Am., 66, 1081 (1976).

(102) Voigtman, E.; Winefordner, J.D.; Appl. Spectrosc., 41, 1182 (1987).

(103) Hirschfeld, T.; Appl. Opt., 16, 3070 (1977).

(104) Hirschfeld, T.; Appl. Spectrosc., 33, 525 (1979).

(105) Hirschfeld, T.; Appl. Spectrosc., 39, 1086 (1985).

(106) Faires, L.M.; J. Anal. Atom. Spectrom., 2, 585 (1987).

(107) Sakai, H.; and Murphy, R.E.; J. Opt. Soc. Am., 60, 422-423 (1970).

(108) Natale, V.; Ventura, G.; Appl. Opt., 23, 2052 (1984).

(109) Knacke, R.F.; Appl. Opt., 17, 684 (1978).

(110) Luc, P.; Gerstenkorn, S.; Appl. Opt., 17, 1327 (1978).

(111) Emonds, J.G.M.; A High Resolution Fourier Transform Spectrometer For the Visible, PhD Dissertation, Utrecht, (1981).

BIOGRAPHICAL SKETCH

Thomas Joseph John Manning was born to James C. and Bette Anne Manning on January 27, 1961. He is of Irish-Catholic decent. He was reared on Staten Island, New York, in an area called Pleasant Plains. He attended St. Joseph and St. Thomas grammar school.

He attended Monsignor Farrell H.S. (1975-1979), an all boys high school. In addition to academics, he spent much time wrestling for his high school and the New York Athletic Club (winner of many national AAU titles). He then spent a semester at Wagner College night school. The next 1.75 years were spent at Clemson University. Working, wrestling, studying and growing up all took time. He then returned to Staten Island and worked at the group home on Roe Street. A group home for PINS (People in need of supervision). Sixteen year old boys who got busted but were not sent to jail. This was a real experience.

In 1982 Thomas J. Manning moved to Charleston, S.C., and attended the College of Charleston (8/82-5/85). He obtained a B.S. in chemistry. He was positively influenced by the faculty at the College of Charleston (Dr. J. Deavor in particular) to attend graduate school. He worked at the

Medical University of South Carolina as a technician (producing his first publication), the bookstore with Carl (RIP) and Spanky's bar as a bouncer and bartender. He also spent a summer working with Geoff Coleman, Vince, and Leigh at the University of Alabama on a chemistry fellowship.

He then entered the University of Florida for graduate school (1985-1990). For a variety of reasons he became disenchanted with graduate school. On many occasions politics and favoritism played the greatest role in success. Ken Spears proved to be the definitive case. On the verge of leaving, he spent a summer at Los Alamos National Lab working with Mike Parsons, Byron Palmer, Doug Hof, and Larry Layman on the Los Alamos Fourier Transform Facility. This changed his outlook on science to what it had been during his undergraduate days. He stuck it out at LANL and UF till he reached this point. During his stay at UF he became president of the scuba diving club and ran a lot of long races. Arlene Reynaldos has recently become an important part of his life. At the moment of writing this he is headed to West Virginia University to work with Ray Lovett in the general area of trace atomic spectroscopy.

I certify that I have read this study and that in my opinion it conforms to acceptable standards of scholarly presentation and is fully adequate, in scope and quality, as a dissertation for the degree of Doctor of Philosophy.

James D. Winefordner, Chairman
Graduate Research Professor
of Chemistry

I certify that I have read this study and that in my opinion it conforms to acceptable standards of scholarly presentation and is fully adequate, in scope and quality, as a dissertation for the degree of Doctor of Philosophy.

Richard A. Yost
Professor of Chemistry

I certify that I have read this study and that in my opinion it conforms to acceptable standards of scholarly presentation and is fully adequate, in scope and quality, as a dissertation for the degree of Doctor of Philosophy.

Vaneica Y. Young
Associate Professor of Chemistry

I certify that I have read this study and that in my opinion it conforms to acceptable standards of scholarly presentation and is fully adequate, in scope and quality, as a dissertation for the degree of Doctor of Philosophy.

Anna Brajter-Toth
Associate Professor of Chemistry

I certify that I have read this study and that in my opinion it conforms to acceptable standards of scholarly presentation and is fully adequate, in scope and quality, as a dissertation for the degree of Doctor of Philosophy.

James H. Hunter

James H. Hunter
Professor of Astronomy

This dissertation was submitted to the Graduate Faculty of the Department of Chemistry in the College of Liberal Arts and Sciences and to the Graduate School and was accepted as partial fulfillment of the requirements for the degree of Doctor of Philosophy.

August, 1990

Dean, Graduate School

UNIVERSITY OF FLORIDA
3 1262 08553 8311